Volume 11
Number 42
14 November 2020
Pages 6711-6854

Polymer Chemistry

rsc.li/polymers

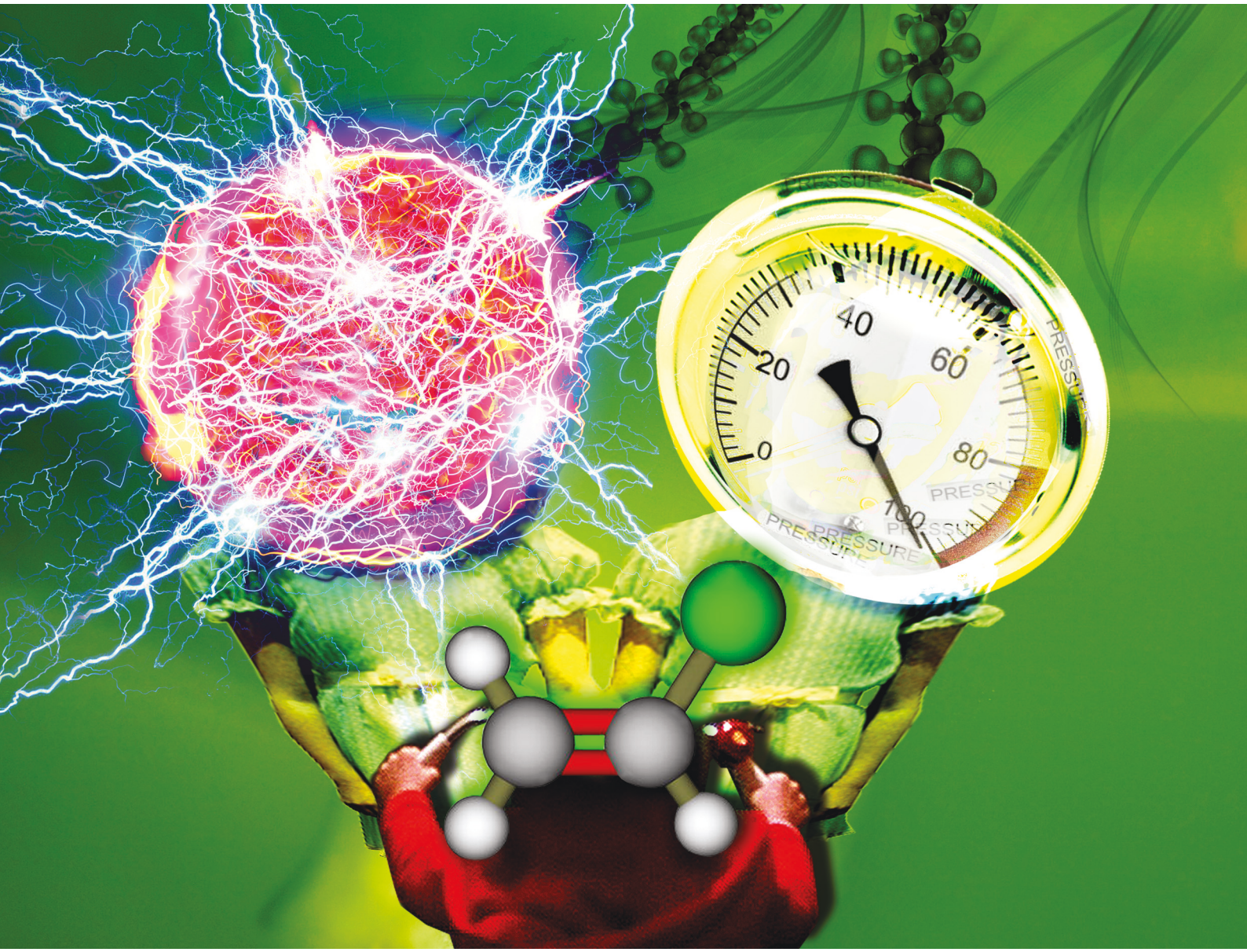

ISSN 1759-9962

ROYAL SOCIETY OF CHEMISTRY

PAPER
Abdirisak A. Isse, Jorge F. J. Coelho *et al.*
Under pressure: electrochemically-mediated atom transfer radical polymerization of vinyl chloride

Polymer Chemistry

ROYAL SOCIETY OF CHEMISTRY

PAPER

View Article Online
View Journal | View Issue

Cite this: *Polym. Chem.*, 2020, **11**, 6745

Under pressure: electrochemically-mediated atom transfer radical polymerization of vinyl chloride†

Francesco De Bon,[a,b] Diana C. M. Ribeiro,[a] Carlos M. R. Abreu,[a] Rafael A. C. Rebelo,[a] Abdirisak A. Isse,*[b] Arménio C. Serra,[a] Armando Gennaro,[b] Krzysztof Matyjaszewski[c] and Jorge F. J. Coelho*[a]

Received 12th July 2020,
Accepted 7th September 2020

DOI: 10.1039/d0py00995d

rsc.li/polymers

The stringent control over the polymerization of less activated monomers remains one major challenge for Reversible Deactivation Radical Polymerizations (RDRP), including Atom Transfer Radical Polymerization (ATRP). Electrochemically mediated ATRP (eATRP) of a gaseous monomer, vinyl chloride (VC), was successfully achieved for the first time using a stainless-steel 304 (SS304) electrochemical reactor equipped with a simplified electrochemical setup. Controlled polymerizations were confirmed by the good agreement between theoretical and measured molecular weights, as well as the relatively narrow molecular weight distributions. Preservation of chain-end fidelity was verified by chain extension experiments, yielding poly(vinyl chloride) (PVC) homopolymers, block and statistical copolymers. The possibility of synthesizing PVC by *e*ATRP is a promising alternative to afford cleaner (co)polymers, with low catalyst concentration. The metal body of the reactor was also successfully used as a cathode. The setup proposed in this contribution opens an avenue for the polymerization of other gaseous monomers.

Introduction

Atom Transfer Radical Polymerization (ATRP) is amply recognized as a very powerful and robust Reversible Deactivation Radical Polymerization (RDRP) method.[1,2] It enables advanced macromolecular engineering by affording (co)polymers with predetermined molecular weights, low dispersity ($Đ$) and precise architectures. During the last 25 years, ATRP has been achieved with various transition metals (or photoredox) catalysts, but copper-catalyzed ATRP (Cu-ATRP) is still the most extensively used, being tolerant to a very wide range of monomers, functionalities, initiators and solvents.[3–21] In Cu-ATRP, the control of the polymerization is driven by the dynamic activation/deactivation equilibrium between a $[Cu^{I}L]^{+}/[X\text{-}Cu^{II}L]^{+}$ redox couple, where L is typically a nitrogen ligand and X = Br, Cl. In electrochemically mediated ATRP (*e*ATRP),[22–30] the Cu^{I} activator complex is (re)generated by electroreduction of Cu^{II} at a working electrode (WE), according to Scheme 1.

Scheme 1 shows the mechanism of *e*ATRP in the presence of a Cu catalyst. The polymerization begins with an air-stable Cu^{II} complex in solution, that is reduced at WE to generate the Cu^{I} activator complex, $[Cu^{I}L]^{+}$. This reacts with an alkyl halide, either molecular initiator (RX) or a (macro)alkyl halide initiator (P_n-X) reforming again the deactivator complex $[X\text{-}Cu^{II}L]^{+}$ and a carbon radical, that adds a few monomer molecules before being again deactivated by $[X\text{-}Cu^{II}L]^{+}$, regenerating $[Cu^{I}L]^{+}$ and the corresponding dormant polymer chain. Equilibrium con-

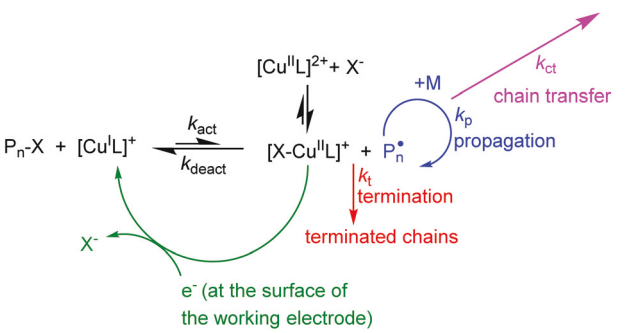

Scheme 1 Mechanism of copper-catalyzed ATRP with regeneration of the activator complex by external electrochemical control. Electroreduction of $[XCu^{II}L]^{+}$ occurs at the surface of the working electrode.

[a]*University of Coimbra, Centre for Mechanical Engineering, Materials and Processes, Department of Chemical Engineering, Rua Sílvio Lima-Polo II, 3030-790 Coimbra, Portugal. E-mail: jcoelho@eq.uc.pt*
[b]*Department of Chemical Sciences, University of Padova, Via Marzolo 1, 35131 Padova, Italy.. E-mail: abdirisak.ahmedisse@unipd.it*
[c]*Department of Materials Science & Engineering, Carnegie Mellon University, 5000 Forbes Avenue, Pittsburgh, PA, USA*

† Electronic supplementary information (ESI) available: Experimental procedures and materials, comparison of different ATRP techniques and blank tests, profiles of $E_{WE} - E_{CE}$ *vs.* time recorded during galvanostatic experiments, NMR spectra and SEC traces of PVC and its copolymers, description of the reactor. See DOI: 10.1039/d0py00995d

stants ($K_{ATRP} = k_{act}/k_{deact}$, Scheme 1) should be strongly shifted to the left, to keep radical concentration low and retain chain-end functionality. In organic solvents, typically $K_{ATRP} < 10^{-4}$ and because of temperature,[3] pressure,[5,6,31–34] solvent,[35] polymer chain-end and, and most of all, ligand structure,[8,36] equilibrium constants span over 8–9 orders of magnitude. The electrochemical stimulus has the unique advantage of reducing the starting Cu^{II} species without by-products since electrons (*i.e.* applied current or potential) are used *in lieu* of chemical reducing agents. Additionally, the ratio between Cu^{II} deactivator and Cu^{I} activator species is a function of the applied potential or current, according to Nernst equation. Therefore, *e*ATRP can be finely tuned by modulating the electrochemical stimulus. It was already applied to several monomers in organic solvents, water (at both neutral and very acidic pH), oil-in-water mini-emulsion, ionic liquids and for the ultrasensitive detection of glucose. Also, *e*ATRP has been successfully triggered from surfaces, or by using Fe-based catalysts or pseudo-halides.[22,23,25,27,28,37–49]

Classically, *e*ATRP is triggered inside electrochemical glass cells with a three-electrode setup: two platinum electrodes serving as cathode (working electrode, WE) and anode (counter electrode, CE) and a reference electrode (RE), which can be a saturated calomel electrode or an $Ag|AgI|I^-$ quasi-reference electrode.[29] All electrodes are in electric contact with the polymerization mixtures. Common CEs and REs contain porous frits and salt bridges of methylcellulose avoiding the direct contact between the sensitive element and the solution. Unfortunately, this setup cannot be used with gaseous monomers because common CEs and REs are not able to retain the pressure and may in the end collapse or explode. Potentiostatic electrolysis, *i.e.* (re)generating the catalyst at a fixed potential (E_{app}) is the most common electrosynthesis. Nevertheless, galvanostatic electrolysis has emerged in the last years. Indeed, galvanostatic regeneration of copper complexes is more intuitive because it is driven by a series of currents.[50] Various developments towards simplifying *e*ATRP setup and making the process cost-effective and more user-friendly have recently been achieved, including Pt replacement with economically affordable electrodic materials (like Ni, SS304 and NiCr alloys).[26,38,51–55] To sustain and confine pressure, robust electrodes such as bulk metals are the most convenient and useful choices. The above-mentioned non-noble metal cathodes and anodes have already been successfully applied in *e*ATRP. Among them, stainless-steel 304 (SS304) cathodes and sacrificial aluminum anodes performed well in galvanostatic *e*ATRP of *n*-butyl acrylate (*n*-BA) and oligo(ethylene oxide) methyl ether methacrylate ($OEOMA_{500}$) in DMF and water, respectively, as well as in a pioneering laboratory scale-up study using a dedicated SS304 electrochemical reactor.[52,55,56] Galvanostatic electrolysis is however not free of drawbacks: the applied potential becomes function also of the stirring rate, and the electrochemical control is less stringent than a potentiostatic one, still however robust enough to avoid parasitic electrochemical processes, with properly tuned applied currents. In the case of simplified galvanostatic *e*ATRP, a sacrificial bulk aluminum anode is directly immersed into the working solution. During electrolysis, this anode releases Al^{3+} into the polymerization medium. A complete study of Al^{3+} effects on copper-catalyzed *e*ATRP in organic solvents has not yet been reported. It has been shown, however, that Al^{3+} competes with Cu ions for Me_6TREN in DMF, undermining the polymerization unless an excess of ligand is used to coordinate all electrogenerated Al^{3+} ions. As a precaution, a ligand excess was always added to the polymerization mixture to avoid all possible interference caused by Al^{3+} release.

For a successful ATRP, the activation rate constant (k_{act}) needs to be high, while the deactivation rate constant (k_{deact}) should be much larger to provide the proper control over the polymerization while allowing a reasonable polymerization rate. For this reason, the controlled polymerization of non-activated monomers such as vinyl chloride (VC) remains a very important challenge, due to the inability of most catalysts to mediate the dynamic of activation/deactivation.[57] The polymerization of non-activated monomer by *e*ATRP, generally referred as Less Activated Monomers (LAMs), has been indeed highlighted as "one of the next exciting direction in the area".[58] The dormant species of such "special" monomers exhibit lower activation rate constant (usually $k_{act} < 10^1$–10^3 M^{-1} s^{-1}) and relatively low propagation rate constant (k_p of VC = 5400 ± 1500 M^{-1} s^{-1} at 25 °C), but still much larger than methyl methacrylate or styrene.[57] Indeed, often a LAM forms much reactive radicals and has higher k_p, like in the case of methyl acrylate *vs.* methyl methacrylate.[59,60] Furthermore, VC exhibits also one of the largest chain transfer constants to monomer ($k_{ct}^M = 22 \times 10^{-4}$ M^{-1} s^{-1} at T = 50 °C) among all vinyl monomers (for instance, $k_{ct}^M = (0.35–0.78) \times 10^{-4}$ M^{-1} s^{-1}, $(0.25–4.5) \times 10^{-4}$ M^{-1} s^{-1} and $(0.2–0.9) \times 10^{-4}$ M^{-1} s^{-1} for styrene, vinyl acetate and ethyl acrylate, respectively, at T = 50 °C).[57,61] Chain transfer is a parasitic reaction by which the radical of a growing chain is transferred to another molecule leading to the formation of structural defects, and to the reducing of the molecular weight of the final polymer. It is believed however that for PVC there is no direct abstraction of growing radical as it happens for other monomers.

The controlled polymerization of VC has been reported using different RDRP methods,[62] including: Single Electron Transfer Degenerative chain Transfer Living Radical Polymerization (SET-DTLRP),[63] Cobalt-Mediated Radical Polymerization (CMRP),[64] Nitroxide-Mediated Polymerization (NMP),[65,66] Supplemental Activator and Reducing Agent Atom Transfer Radical Polymerization (SARA ATRP),[67–70] Activators Regenerated by Electron Transfer Atom Transfer Radical Polymerization (ARGET),[71] Reversible Addition–Fragmentation chain Transfer polymerization (RAFT)[66,72] and Macromolecular Design *via* the Interchange of Xanthate (MADIX).[73] In ATRP, the preferred solvent for VC polymerization is DMSO, which is one of the few able to dissolve PVC and one of the first historically used for VC controlled radical polymerization.[74–78] Until now, RDRP of VC by electrochemical methods has never been attempted, due to several issues associated to the intrinsic characteristics of VC (boiling point

= −13.5 °C) and the special equipment required. Ordinary electrochemical glassware does not sustain the pressure of VC, comprised between 5–6 bar at T = 40–45 °C.[79,80] This temperature has been found to be an optimal compromise between the rate of polymerization and formation of PVC structural defects (allyl and tertiary alkyl chlorides).[81–83] To overcome the pressure issue, a robust SS304 electrochemical reactor was used. This strategy permitted on one hand to confine the monomer and its pressure, ensuring safe operations throughout all experiments, and on the other hand to apply the galvanostatic polymerization conditions already successfully applied for other monomers.[52]

Here, the polymerization of VC was studied by exploring relatively a large set of experimental conditions, using a conventional platinum electrode: homo and copolymerization, different ligands, different initiators (including multifunctional alkyl halides), and different current densities (Scheme 2). At the end, use of the SS304 scaffold of the reactor as a cathode was attempted to fully resemble a prototype of industrial polymerization reactor, with a further electrochemical simplification.

Contrarily to SARA ATRP, where comproportionation is the driving force of $[Cu^{I}L]^{+}$ regeneration,[84–86] here active $[Cu^{I}L]^{+}$ is (re)generated by application of an electrical stimulus, which reduces the ternary complex $[X–Cu^{II}L]^{+}$. $[Cu^{II}TREN]^{2+}$ (TREN = tris(2-aminoethyl)amine) was chosen as a catalyst, based on the literature, considering its ability to mediate SARA ATRP of VC as well as of other monomers.[67–71] Despite the electrochemical advantages introduced in the last years and since *e*ATRP of VC has never been attempted before, a traditional Pt mesh (estimated geometrical A = 6 cm^2) was used as WE for most experiments. Also, as precaution the cell configuration was undivided, with aluminum CE directly immersed into the solution. Since usual reference electrodes cannot sustain high pressure, electrochemical investigations in the SS304 reactor were not performed in presence of VC. Nevertheless, electrochemical characterizations of PVC obtained by conventional radical polymerization (RP) or by *e*ATRP were instead carried out by cyclic voltammetry, in the presence or in the absence of the catalyst. This work describes the first electrochemically mediated ATRP of a LAM under pressure. The proposed setup can potentially help to polymerize several other monomers with a simplified equipment under pressure. The possibility of using the steel scaffold of the reactor as a cathode, combined with an even more simplified electrochemical setup opens new horizons for a further simplification of *e*ATRP.

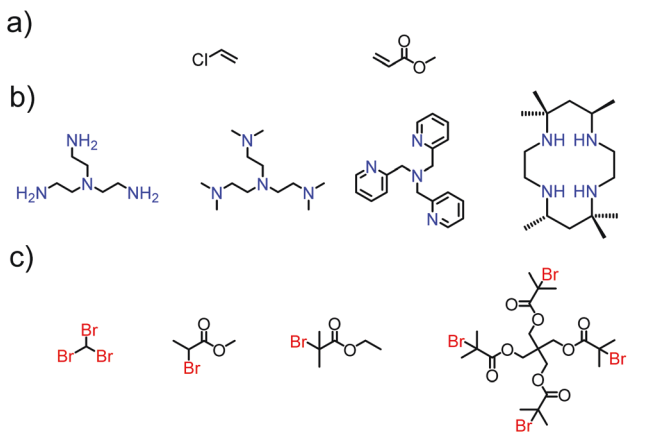

Scheme 2 Summary of monomers (vinyl chloride and methyl acrylate, (a), ligands from left to right (tris(2-aminoethyl)amine (TREN), tris(2-dimethylaminoethyl)amine (Me_6TREN), tris(2-pyridylmethyl)amine (TPMA) and 5,5,7,12,12,14-hexamethyl-1,4,8,11-tetraazacyclotetradecane, (Me_6Cyclam) (b) and initiators from left to right (bromoform, methyl 2-bromopropionate, ethyl 2-bromoisobutyrate and pentaerythritol tetrakis(2-bromoisobutyrate), (c) used in this study.

Experimental

Safety consideration

Vinyl chloride is a hazardous, flammable, toxic and carcinogenic gas and should be handled with extreme care. A gas detector should be always used while operating with VC in a well-ventilated fume hood. However, its polymer is nowhere near as acutely toxic as the monomer.

Materials

Methyl acrylate (MA, 99% stabilized; Acros) was passed through an alumina column before use to remove the radical inhibitors. Vinyl chloride (VC, 99%) was kindly supplied by CIRES Lda, Portugal. Copper(II) bromide ($CuBr_2$, +99% extra pure, anhydrous; Acros), copper wire (Cu^0, >99.999% trace metal basis, Alfa Aesar), deuterated chloroform ($CDCl_3$ + 1% tetramethylsilane (TMS); Euriso-top), deuterated tetrahydrofuran (THF-d_8, 99.5%; Euriso-top), bromoform ($CHBr_3$, +99% stabilized with ethanol; Acros), tris(2-aminoethyl)amine (TREN, 96%; Acros), pentaerythritol tetrakis(2-bromoisobutyrate) (EBiB-4f, Sigma-Aldrich 97%), copper(II) trifluromethanesulfonate ($Cu(OTf)_2$, Alfa Aesar, 98%), methyl 2-bromopropionate (Sigma Aldrich, 98%), ethyl 2-bromoisobutyrate (Acros Organics, 98%), copper(I) tetrakis(acetonitrile) tetrafluoroborate ($Cu(I)(CH_3CN)_4BF_4$, Sigma Aldrich, 99%), (2,2,6,6-tetramethylpiperidin-1-yl)oxidanyl (TEMPO, Sigma Aldrich, 98%) and 1,1-bromochloroethane (Alfa Aesar, 98%) were used as received. Tetraethylammonium tetrafluoroborate (Et_4NBF_4, Alfa Aesar, 98%) was recrystallized twice from ethanol and dried in a vacuum oven at 40 °C, over weekend. Dimethyl sulfoxide (99.9%; Fischer Scientific) was distilled under vacuum from CaH_2 and stored over molecular sieves. High-performance liquid chromatography (HPLC) grade THF (Panreac) was filtered (0.2 μm filter) under reduced pressure before use. Metallic copper was washed with aqueous HCl in methanol and subsequently rinsed with acetone and dried under a stream of nitrogen following the literature procedures. A stock solution (*ca.* 0.2 M in CH_3CN) of tetrakis(acetonitrile) copper(I) tetrafluoroborate (Cu^{I} $(MeCN)_4BF_4$) was prepared in a drybox and standardized by spectrophotometric analysis, using 2,9-dimethyl-1,10-phenanthroline as a specific ligand (ε = 8458 M^{-1} cm^{-1}) in a 2-fold excess with respect to the metal.

Methods

The chromatographic parameters of the samples were determined using high performance size exclusion chromatography HPSEC; Viscotek (Viscotek TDAmax) with a differential viscometer (DV); right-angle laser-light scattering (RALLS, Viscotek); low-angle laser-light scattering (LALLS, Viscotek) and refractive index (RI) detectors. The column set consisted of a PL 10 mm guard column (50 × 7.5 mm^2) followed by one Viscotek Tguard column (8 μm), one Viscotek T2000 column (6 μm), one Viscotek T3000 column (6 μm) and one Viscotek LT4000L column (7 μm). HPLC dual piston pump was set with a flow rate of 1 mL min^{-1}. The eluent (THF) was previously filtered through a 0.2 μm filter. The system was also equipped with an on-line degasser. The columns were thermostated at 30 °C using an Elder CH-150 heater. Before the injection (100 μL), the samples were filtered through a polytetrafluoroethylene (PTFE) membrane with 200 nm pores. The system was calibrated with narrow PS standards. The d*n*/d*c* was determined as 0.063 for PMA, 0.105 for poly(vinyl chloride) (PVC) and 0.185 for polystyrene standards (PS). Molecular weight (M_n^{SEC}) and dispersity ($Đ$) of the synthesized polymers were determined by multi-detectors calibration. ^{1}H-NMR spectra of reaction mixture samples were recorded on a Bruker Avance III 400 MHz spectrometer, with a 5 mm TIX triple resonance detection probe, in $CDCl_3$, DMSO-d_6, or THF-d_8 with 1% Me_4Si (TMS) as an internal standard. The composition of copolymers was determined by integration of characteristic signals (OCH_3 singlet at δ_H = 3.65 ppm for PMA and –CH–Cl signals at δ_H = 3.80–4.30 ppm for PVC).

Voltammetric experiments were carried out in a three-electrode cell with a double wall jacket through which water from a thermostated bath (Thermo Scientific, HAAKE SC100) was circulated. All experiments were carried out at 40 ± 0.1 °C. An Autolab PGSTAT30 potentiostat/galvanostat, a μAutolab Type II (EcoChemie, The Netherlands) run by a PC with GPES software and a Bio-Logic SP-150 Potentiostat/Galvanostat/EIS instrument run by a PC with EC-Lab software were used for electrochemical analysis or polymerizations. The working electrode used in voltammetric analysis was a 3 mm diameter GC disk (Tokai GC-20), whereas the counter and reference electrodes were a Pt ring and Ag|AgI|0.1 M *n*-Bu_4NI in DMF, respectively. Prior to each experiment the working electrode surface was cleaned by polishing with a 0.25 μm diamond paste, followed by ultrasonic rinsing in ethanol for 5 min. At the end of each experiment the potential of the reference electrode was calibrated against the ferrocenium/ferrocene couple or SCE: E^θ = 0.391 V *vs.* SCE in CH_3CN, and E^θ = 0.449 V *vs.* SCE in DMSO.[87] the determination of $k_{act} < 10^3$ M^{-1} s^{-1} and k_{disp}, the GC working electrode was connected to a rotating disk electrode (RDE, Metrohm Autolab).

Procedures

Procedure for voltammetric analysis of $[Cu^{II}(L)]^{2+}$ and $[Cu^{II}(L)Br]^+$. Prior to use, the electrochemical cell was cleaned with acetone and dried in an oven at ~60 °C. Then, the three electrodes were put into the cell and the remaining necks were closed with PTFE caps. The supporting electrolyte, Et_4NBF_4 (0.217 g, 1.0 mmol), a stirring bar and 10 mL of anhydrous solvent were added to the cell under nitrogen flow. Then, $Cu^{II}(OTf)_2$ (3.61 mg, 0.01 mmol) and the ligand ([L]/[Cu] = 1.0) were added to the solution. After recording a CV at a scan rate of 0.2 V s^{-1}, Et_4NBr (2.32 mg, 0.012 mmol) was added in solution and another CV was recorded. All complexes exhibited a quasi-reversible voltammetric response, thus E^θ was obtained as the semi-sum of anodic and cathodic peak potentials, *i.e.* $E^\theta \approx E_{1/2} = (E_{pa} + E_{pc})/2$.

Procedure for k_{act} determination by rotating disc electrode (RDE). Prior to use, the electrochemical cell was cleaned with acetone and dried in an oven at ~60 °C. Then, the three electrodes were put into the cell and the remaining necks were closed with PTFE caps. The supporting electrolyte, Et_4NBF_4 (0.325 g, 1.5 mmol), the stirring bar and 15 mL of anhydrous solvent were added to the cell under argon flow. In the experiments for k_{act} determination, TEMPO (0.117 g, 0.75 mmol) was also added into the cell. The amount of TEMPO was 10- to 20-fold in excess over Cu(I), to assure that all generated radicals were immediately trapped by the nitroxide. After degassing the solution for about 30 minutes, a known amount of a Cu(I) solution in CH_3CN was withdrawn with a syringe from the stock solution, under inert atmosphere, and injected into the cell. The initiator was injected into the cell few seconds after Cu(I).

Activation of working electrodes and cleaning of the reactor. Before each *e*ATRP, the platinum gauze used as the working electrode was cleaned by ultrasonication in THF for 10 minutes to remove any trace of PVC. Afterwards, it was activated by ultrasonication in concentrated nitric acid (60%) for 10 minutes to remove any contaminant on the surface. The electrode was then rinsed abundantly with double distilled water and acetone. The aluminum rod, which served as anode, was polished at the beginning of this study with fine grain grit paper to remove oxides and all possible contaminants, washed with diluted hydrochloric acid (~0.05 M) and rinsed with abundant double distilled water and acetone. Before each experiment, the surface was washed with THF, water, acetone and then dried in the air. The SS304 reactor was washed first with THF followed by acetone to remove any trace of PVC or organics and then with a diluted solution of nitric acid (~0.025 M) to remove any trace of copper. The final rinsing consisted of washing with abundant distilled water and acetone.

Loading of the reactor

Loading of vinyl chloride. The body of the reactor, containing the stirring bar, was cooled by immersion in liquid nitrogen. Then pre-condensed vinyl chloride (5 mL, 4.55 g, 72.88 mmol) was poured inside and frozen immediately. The exact amount of VC was determined gravimetrically. The head was mounted and sealed, by closing tightly the four threaded screws; the reactor was then submitted to 5–10 vacuum/N_2

cycles. All operations were performed keeping the body of the reactor cooled in liquid nitrogen.

Loading of the working solution. A pre-degassed 5 mL solution of DMSO, containing 1×10^{-3} M $CuBr_2$ (2.23 mg, 0.01 mmol), 2×10^{-3} M tris(2-aminoethyl)amine (TREN, 2.93 mg, 0.02 mmol), 1.5×10^{-2} M bromoform ($CHBr_3$, 37.91 mg, 0.15 mmol) and 10^{-1} M tetraethylammonium tetrafluoroborate (Et_4NBF_4, 0.217 g, 1 mmol) was inserted through the degassing valve *via* deoxygenated syringe under N_2 flow, while the body reactor was immersed in liquid nitrogen. Afterwards, the reactor was submitted to fifteen vacuum/N_2 cycles. After the last cycle, the valve was closed, and the reactor was heated to room temperature with a heat-gun.

Typical eATRP of vinyl chloride. The reactor was placed in a water bath at T = 40 °C with all the body immersed in water and let to equilibrate for 30 minutes, with stirring set at 700 rpm. After that, the electric plugs were connected to the electrodes to record the evolution of $E_{WE} - E_{CE}$ with time. The desired electrolysis program was finally applied (see Fig. 7).

Typical synthesis of PVC by SARA ATRP. A 50 mL Ace glass 8645#15 pressure tube, equipped with bushing and plunger valve, was charged with a degassed mixture of $CHBr_3$ (13.1 μL, 0.15 mmol), $CuBr_2$ (2.23 mg, 0.01 mmol), TREN (3.0 μL, 0.2 mmol) and DMSO (5 mL). The tube was then frozen in liquid nitrogen. Precondensed VC (5 mL, 72.88 mmol) was added liquid to the tube. After VC was frozen completely, a stirring bar wrapped with a Cu^0 wire (l = 5 cm, d = 1 mm), which was previously activated with a HCl/MeOH solution (1/3 v/v) was added. The exact amount of VC was determined gravimetrically. The tube was closed, submerged in liquid nitrogen, and degassed through the plunger valve by applying vacuum cycles and filling the tube with N_2 about 15 times. The valve was closed, and the tube reactor was placed in a water bath at 40 °C with stirring (700 rpm). After 6 h, the reaction was stopped by plunging the tube into cold water. The tube was slowly opened, the excess VC was vented off, and the mixture was precipitated into methanol. The polymer was separated by filtration, washed with water, and dried in a vacuum oven until reaching constant weight.

Recovery of PVC-Br. At the end of electrochemical polymerizations, the reactor was cooled to room temperature and the degassing valve was opened to vent off unreacted vinyl chloride, under stirring. Then the head was disconnected from the body and the polymerization mixture was taken up with THF and precipitated in cold methanol, washed three times with methanol, then water and dried in a vacuum oven until reaching constant weight.

Chain extension with methyl acrylate. To a round bottom flask were added PVC-Br (M_n = 8900, $Đ$ = 1.70, 178 mg, 0.02 mmol), DMSO (5 mL), methyl acrylate (MA, 5 mL, 55.2 mmol), $CuBr_2$ (2.23 mg, 0.01 mmol) and TREN (2.93 mg, 0.02 mmol). The solution was bubbled with nitrogen for 30 minutes. Next it was transferred, *via* degassed syringe, to a deoxygenated Schlenk flask containing a stirring bar wrapped with a previously activated Cu^0 wire (d = 1 mm, l = 5 cm). The polymerization was triggered at T = 40 °C with 700 rpm stirring. After 10 min, the Schlenk was opened to air to quench the reaction. Samples for NMR and SEC were withdrawn.

Results and discussion

Electrochemical characterizations

The electrochemical behavior of copper complexes with TREN and Me_6TREN was analyzed in DMSO (Fig. 1). Before starting the study of VC polymerization, cyclic voltammetry of the system was performed on a glassy carbon (GC) disk, to measure the formal reduction potential of the copper complexes. A reversible peak couple attributed to the reversible reduction of $[BrCu^{II}L]^+$ to $[BrCu^{I}L]$ (L = TREN, Me_6TREN) was observed in the absence of initiator. The same for $Cu(OTf)_2$, which is solvated by DMSO molecules in solution (S), its reversible peak couple is attributed to the reversible reduction of Cu(II) to Cu(I). The standard redox potentials ($E_{1/2}$ *vs.* SCE in DMSO) are: −0.479 V, −0.347 V and 0.003 V for $[BrCu^{II}TREN]^+$, $[BrCu^{II}Me_6TREN]^+$ and solvated Cu(II) cations respectively.

Electrochemical investigation in the presence of $[Cu^{II}TREN]^{2+}$ was performed prior to electrochemically mediated ATRP. Although the stability constants of the electrogenerated Cu(I) complexes, $[Cu^{I}TREN]^+$ and $[XCu^{I}TREN]$, in DMSO and VC/DMSO are not known, it is likely that $[Cu^{I}TREN]^+$ is the only species present in solution when TREN is the only ligand in solution, whereas both species will be formed in the presence of both TREN and X^-. The general disproportionation reaction of Cu^I species present in solution can be expressed as (eqn (1)):

$$2Cu^{I} \rightleftarrows Cu^{II} + Cu^{0} \quad (1)$$

Kinetics of disproportionation were performed by monitoring the concentration of Cu^I on a rotating disc electrode (RDE), operating at a fixed angular velocity (ω = 2500 rpm) and a constant applied potential of −0.2 V *vs.* SCE. This value is significantly more positive than $E_{1/2}$ of all the relevant copper complexes present in solution (see Fig. 1). Therefore, all Cu^I species undergo oxidation at the electrode. To determine k_{disp} a constant potential was applied to the RDE in a solution containing the ligand but without copper. Cu^I was then intro-

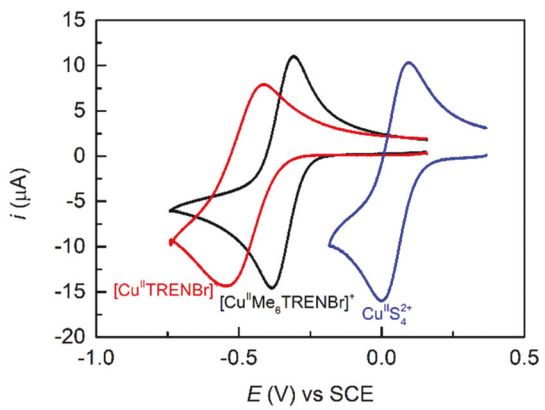

Fig. 1 Cyclic voltammetry of 10^{-3} M $[BrCu^{II}L]^+$ (L = TREN — or Me_6TREN —) and of solvated Cu^{2+} cations from $Cu(OTf)_2$ (—). CV were recorded in DMSO + 0.1 M Et_4NBF_4, at a glassy carbon electrode at v = 0.2 V s^{-1} and T = 40 °C.

duced and immediately an anodic current was observed, which decayed with time owing to the disproportionation reaction. The disproportionation rate constants determined for $[Cu^{I}TREN]^{+}$ in DMSO are summarized in Table 1.

It is worth noting that these disproportionation experiments did not give highly reproducible results, therefore all reported k_{disp} values were obtained as the average of at least two experiments. According to the data of Table 1, disproportionation of $[Cu^{I}TREN]^{+}$ in DMSO is not a fast reaction, which contradicts the mechanistic claims of SET-LRP.[76,88–90] It is important to note that only the first 150 s of the reaction were analyzed with the linear regression to determine k_{disp} (Fig. 2). This short reaction time was chosen to avoid possible contribution of the inverse comproportionation reaction to the overall reaction rate and to prevent significant consumption of Cu^{I} by the oxidation process at the electrode. Both comproportionation and Cu^{I} consumption by electrooxidation become relevant at much longer times.

Once determined that disproportionation is not a fast reaction, kinetic analysis was performed to determine k_{act} of the model chain-end in the presence of the catalyst. The terminal unit model for VC is 1-bromo-1-chloroethane ($CH_3CHClBr$, VC-Br, Fig. 3), a geminal alkyl dihalide.

The reactions between $[Cu^{I}L]^{+}$ and RX are fast, but the ATRP equilibrium is strongly shifted toward the reactants. Under normal conditions, the fraction of converted Cu^{I} is very low, preventing the possibility of obtaining any kinetic information by simply mixing Cu^{I} and RX. To overcome this difficulty, the radical scavenger 2,2,6,6-tetramethyl-1-piperidinyloxy (TEMPO) was used in a large excess with respect to Cu^{I}, allowing quantitative and irreversible trapping of $R^{\bullet}$. The rate constant of radical trapping by nitroxides is typically close to the diffusion controlled limit,[91] so that the overall process (eqn (2) and (3)) can be irreversible and kinetically controlled by the activation reaction, due to $[Cu^{I}TREN]^{+}$:[92]

$$[Cu^{I}L]^{+} + RX \rightleftarrows [XCu^{II}L]^{+} + R^{\bullet} \quad (2)$$

$$R^{\bullet} + TEMPO \rightleftarrows R\text{-}TEMPO \quad (3)$$

Another important issue that should be considered is that besides activating RX, Cu^{I} is engaged in a disproportionation reaction. Previous kinetic studies comparing the decay rates of Cu^{I} in the absence and presence of RX have shown that RX activation is much faster than disproportionation.[93] The lifetime of Cu^{I} is drastically reduced in the presence of RX; disproportionation reactions require hours to approach equilibrium,

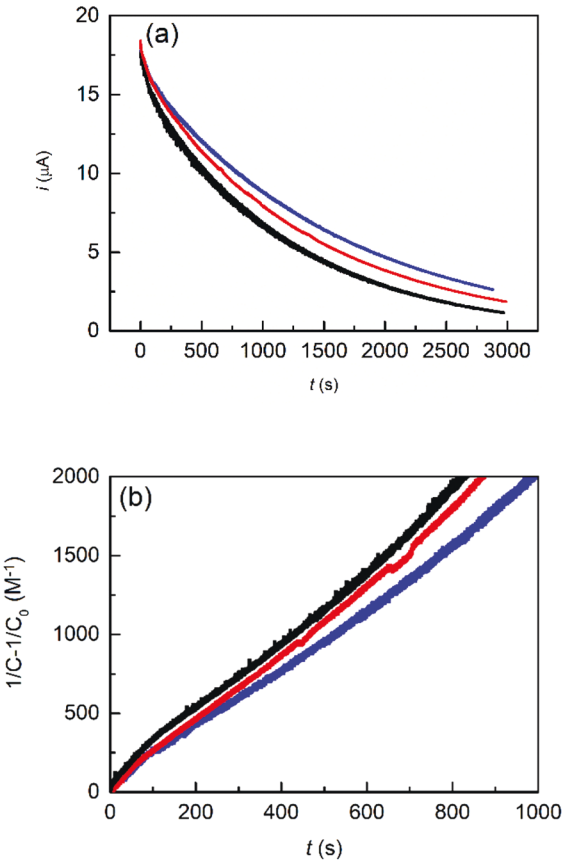

Fig. 2 (a) Decay of limiting current *vs.* time and (b) kinetic determination for k_{disp} in DMSO + 0.1 M Et_4NBF_4: $C_{CuI/TREN}$ = 5 × 10^{-4} M, T = 40 °C, ω_{RDE} = 2500 rpm. Blue: $C_{Br}/C_{TREN}/C_{Cu}$ = 4/2/1; red: $C_{Br}/C_{TREN}/C_{Cu}$ = 0/2/1; black: $C_{Br}/C_{TREN}/C_{Cu}$ = 0/1/1. Interval time analyzed: 150 s. Currents were recorded on rotating GC electrode.

Fig. 3 Structures of VC monomer and of $CH_3CHClBr$ *gem*-dialkyl halide which mimics PVC-Br chain-end.

whilst activation reactions last a few minutes. Therefore, activation kinetics can be monitored following the disappearance of Cu^{I} at a rotating disc electrode (RDE), neglecting the contribution of disproportionation to the rate of Cu^{I} decay. The reaction was studied using equimolar amounts of Cu(I) and RBr, *i.e.* $c_{RBr} = c_{[Cu^{I}L]^{+}}$. Therefore, the rate law becomes (eqn (4)):

$$\frac{1}{C_{Cu(I)}} - \frac{1}{C^{0}_{Cu(I)}} = k_{act}t \quad (4)$$

The results of the activation rate constant experiments are reported in Table 2 and Fig. 4:

Activation by $[Cu^{I}TREN]^{+}$ occurs with k_{act} = 450–800 M^{-1} s^{-1} and, in other words, in the presence of $CH_3CHClBr$, $[Cu^{I}TREN]^{+}$ activates rather C–Br than disproportionating to

Table 1 Disproportionation rate constant (k_{disp}) for $[Cu^{I}TREN]^{+}$ in DMSO + 0.1 M Et_4NBF_4 at T = 40 °C[a]

Entry	C_{TREN} (eq.)	C_{Br^-}[b] (eq.)	C_{Cu} (mM)	k_{disp} (M^{-1} s^{-1})
1	1	0	0.5	1.1
2	2	0	0.5	1.0
3	2	2	0.5	0.9

[a] $C_{Cu(I)}$ = 5 × 10^{-4} M. Accuracy ± 20%. [b] Added as Et_4NBr.

Table 2 Activation rate constant (k_{act}) for the reaction between $[Cu^{I}TREN]^{+}$ and $CH_3CHClBr$ in DMSO + 0.1 M Et_4NBF_4 at T = 25 °C [a]

Entry	C_{Cu} (eq.)	C_{TREN} (eq.)	C_{Br^-} [b] (eq.)	$C_{CH_3CHClBr}$ (eq.)	k_{act} (M^{-1} s^{-1})
1	1	1	0	1	519
2	1	2	0	1	794
3	1	1	2	1	596
4	1	2	2	1	457

[a] $C_{Cu(I)} = 2 \times 10^{-4}$ M, $C_{Cu(I)} : C_{TEMPO} = 1 : 20$. Accuracy ± 5%. [b] Added as Et_4NBr.

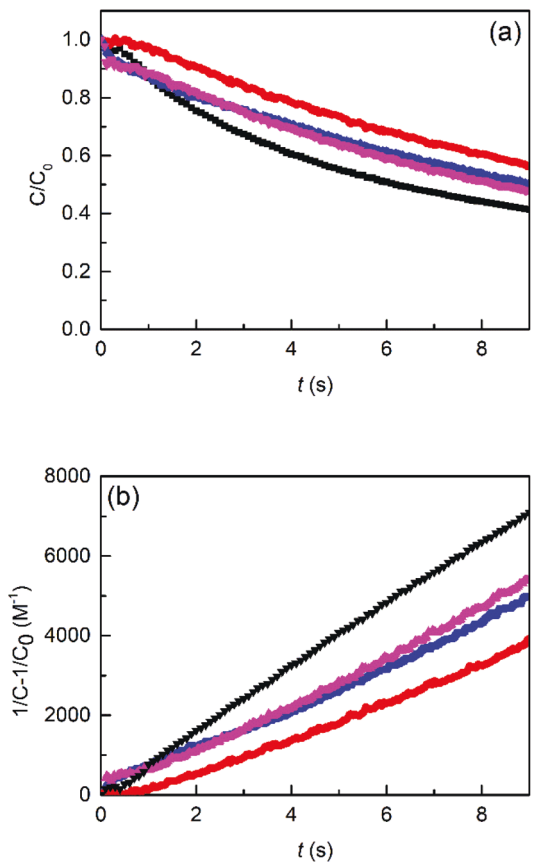

Fig. 4 (a) Decay of 2×10^{-4} M $[Cu^{I}TREN]^{+}$ *vs.* time in the presence of: 2×10^{-4} M VC-Br + 4×10^{-4} M TREN (—); or 2×10^{-4} M VC-Br + 4×10^{-4} M Et_4NBr + 4×10^{-4} M Et_4NBr (—); or 2×10^{-4} M VC-Br (—) + 2×10^{-4} M TREN; or 2×10^{-4} M TREN + 2×10^{-4} M VC-Br + 4×10^{-4} M Et_4NBr (—); (b) data elaboration for k_{act} determination in DMSO + 0.1 M Et_4NBF_4 at 25 °C, according to a second-order rate law; ω_{RDE} = 4000 rpm, analyzed interval time: 9 s. Currents were recorded on a rotating GC electrode.

Cu^0 and Cu(II). Indeed, activation of the alkyl halide by $[Cu^{I}TREN]^{+}$ entails concomitant conversion of the latter to stable $[BrCu^{II}TREN]^{+}$, without formation of metallic copper. Then, the electrochemical response of PVC (either commercial or produced by *e*ATRP) in DMSO was analyzed in the absence of the catalyst. Fig. 5a shows the CV recorded in absence (black line) or in the presence of commercial PVC (red line, DP ≈ 700) and PVC produced by *e*ATRP (blue line, DP = 150) in the oxidation scan. The latter shows the signal of oxidation of bromide ions, probably released due termination events in solution during the polymerization and trapped into the polymer during the recovery procedure of PVC by precipitation. On the opposite direction, reduction of PVC-Br occurs at very negative potentials, near the reduction of the solvent (Fig. 5b). A single irreversible cathodic peak attributed to the reductive cleavage of the terminal C–Br group is observed at $E_p = -3.1$ V. Commercial PVC in DMSO does not show the characteristic peak of C–Br bond reduction, confirming the absence of the functional group in PVC prepared by conventional RP, thus highlighting its non-living behavior.

In a similar manner, the voltammetric response of multifunctional PVC (DP = 765), obtained by *e*ATRP using EBiB-4f (see Table 10 and Fig. 9), was analyzed in the presence of the catalyst in DMSO and compared again to the cyclic voltammetry of a commercial PVC. As can be seen, multifunctional PVC is readily activated by the catalyst: cathodic peak increases while anodic peak decreases due to the onset of *e*ATRP equilibrium (Fig. 6a). No significant modifications are observed if a commercial PVC is instead used (Fig. 6b).

Blank tests

Zerovalent metals (Cu^0, Fe^0, Zn^0 and others) can behave as reducing agents and supplemental activators of dormant alkyl halide species, inducing a non-external unwanted reaction equilibrium. In this work, blank polymerizations were attempted, using the reaction mixture left inside the stainless-steel reactor (SS304 alloy) for 6 hours; no polymerization has occurred. These results indicate that the metal composition of vessel has no effect on the polymerization (see section S1†).

Effect of the ligand structure

To date, the only reported catalyst able to polymerize VC *via* ATRP is $[Cu^{II}TREN]^{2+}$.[62,67–71] This behavior was further confirmed by *e*ATRP. Indeed, if other ligands are used, no polymerization takes place (Table 3).

Cyclic voltammetry unveiled that $[Cu^{I}Me_6TREN]^{+}$ traps 1-chloroethyl radical, forming an organometallic intermediate, which is perhaps inert to the polymerization (see Fig. 13). It is probable that this organometallic species is formed quickly after the generation of the radical and its formation blocks the polymerization. On the other hand, macrocyclic ligands are known to yield copper complexes that are poor deactivators leading to uncontrolled polymerizations.[16,18] This fact was experimentally confirmed by triggering galvanostatic *e*ATRP of MA in DMSO with $[Cu^{II}Me_6Cyclam]^{2+}$ as catalyst: PMA exhibited broad dispersity ($Đ > 2$) after just 10 minutes of reaction, with M_n^{SEC} far higher than M_n (not shown). $[Cu^{II}TPMA]^{2+}$ is instead not sufficiently active for VC terminal, most likely due to the very low k_{act} for the *gem*-dihalide functionality. Indeed, the standard redox potential of this catalyst is considerably more positive than that of $[Cu^{II}Me_6TREN]^{2+}$ or $[Cu^{II}TREN]^{2+}$ and activity of an ATRP catalyst scales with its $E_{1/2}$.[24,94]

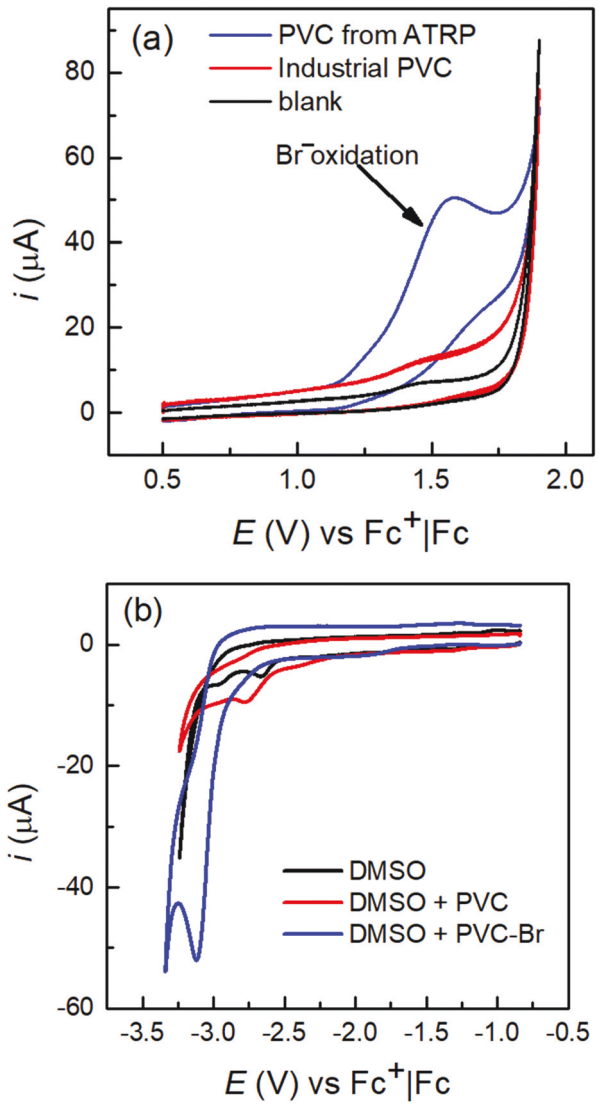

Fig. 5 (a) Cyclic voltammetry of 10^{-3} M PVC (commercial — or obtained by *e*ATRP —) in the oxidation scan; (b) cyclic voltammetry of 10^{-3} M PVC (commercial — or obtained by *e*ATRP —) in the reduction scan. CVs were recorded in DMSO + 0.1 M Et_4NBF_4, at a glassy carbon electrode at v = 0.2 V s^{-1} and T = 40 °C.

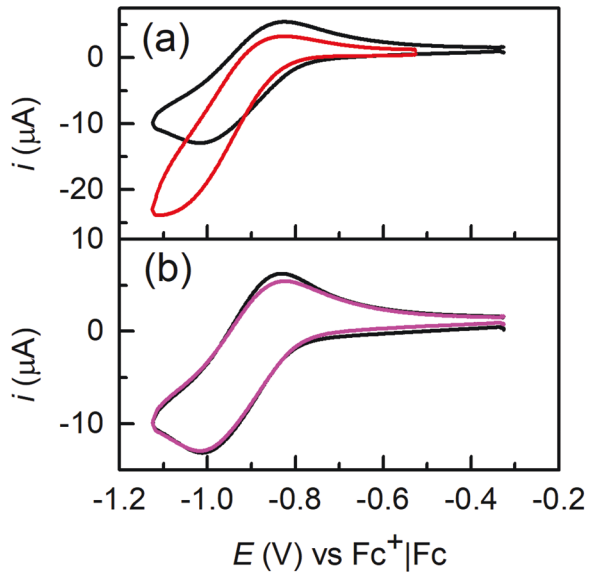

Fig. 6 Cyclic voltammetry of 10^{-3} M $[BrCu^{II}TREN]^+$ in DMSO + 0.1 M Et_4NBF_4 (—) (a) in the presence of 2×10^{-3} M of tetrafunctional PVC-Br (—) or (b) 2×10^{-3} M of commercial PVC obtained by conventional radical polymerization (—). CVs were recorded at a glassy carbon electrode at v = 0.2 V s^{-1} and T = 40 °C.

Effect of the applied current program

The sequence of current/time steps plays a key role during the polymerization. The activator form of the catalyst is (re)generated at WE at a rate imposed by the current feeding. During a galvanostatic electrolysis, the applied potential at WE is free to drift with time to match the imposed current value. Control over molecular distribution is affected by both very fast and very low Cu(I) regeneration rates during *e*ATRP, *i.e.*, fixing very high or very low current. For methyl acrylate (MA), the galvanostatic polymerizations reached the highest conversion and lowest $Đ$ with a multistep electrolysis program (four steps of respectively decreasing current and increasing time), while single step experiments provided very poor results.[52] Galvanostatic electrochemical ATRP of vinyl chloride was started by modifying the electrolysis program, as done for other monomers.[52] Four electrolysis programs composed of five time/current steps were applied to impose a fixed current or simulate the typical decay of i *vs.* t during potentiostatic electrolysis. The current steps were chosen to produce $[Cu^{I}TREN]^+$ at a high rate at the beginning of the polymerization, and then slowly in later stages of the process to simulate the reactivation of Cu^{II} species accumulated by termination events. Most of the experiments were protracted for 6 hours

Table 3 *e*ATRP of 50 vol% VC in DMSO initiated by $CHBr_3$ with different ligands at T = 40 °C [a]

Entry	Ligand	t (h)	M_n^{th}	M_n^{SEC}	$Đ$	Conv. (%)	I_{eff}	Q (C)
1	TREN	6	9400	10 900	1.35	31	0.86	2.95
2	Me_6TREN	6	—	—	—	—	—	2.95
3	TPMA	6	—	—	—	—	—	2.95
4	Me_6Cyclam	6	—	—	—	—	—	2.95

[a] Conversion was determined gravimetrically. $C_{VC} : C_L : C_{Cu} : C_{CHBr_3}$ = 728 : 0.2 : 0.1 : 1.5; V = 10 mL; $C_{Cu} = 10^{-3}$ M, $C_{CHBr_3} = 1.5 \times 10^{-2}$ M. V = 10 mL. Estimated geometrical surface of the Pt electrode = 6 cm^2. Applied current program III (see Fig. 7).

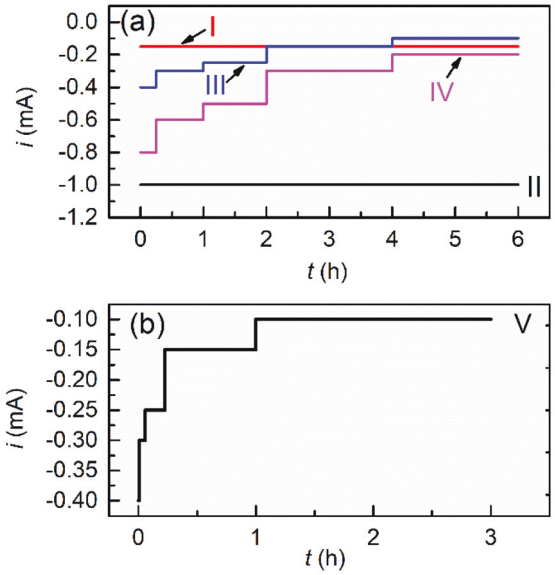

Fig. 7 Electrolysis programs applied during galvanostatic *e*ATRP of vinyl chloride during (a) 6 hours experiments or (b) 3 hours experiments.

and the tested electrolysis programs are illustrated in Fig. 7 and reported below:

1. Single fixed current/time step at $i_{app} = -1.5 \times 10^{-4}$ A ($Q = -3.24$ C);

2. Single fixed current/time step at $i_{app} = -1 \times 10^{-3}$ A ($Q = -21.60$ C);

3. Multistep electrolysis at i_{app} = (−4, −3, −2.5, −1.5 and −1.0) × 10^{-4} A for 300, 600, 2700, 3600 and 14 400 seconds, respectively ($Q = -2.95$ C);

4. Multistep electrolysis at i_{app} = (−8.0, −6.0, −5.0, −3.0 and −1.5) × 10^{-4} A for 300, 600, 2700, 3600 and 14 400 seconds, respectively ($Q = -5.90$ C).

It is worth mentioning that 6 hours experiments were primarily investigated due to the kinetics of polymerization observed for SARA ATRP (Table S1†).[62,68,95] However, 3 hours experiments were chosen only in some selected conditions and the employed electrolysis program was a multistep electrolysis at i_{app} = (−4, −3, −2.5, −1.5 and −1.0) × 10^{-4} A for 30, 180, 600, 2790 and 7200 seconds, respectively (program V, Fig. 7b).

A set of experiments was dedicated to evaluating the effect of different types of electrolysis, as shown in Table 4.

When a -1.5×10^{-4} A constant current was applied, the polymerization occurred, and moderate conversion was obtained with PVC exhibiting quite high $Đ$ (entry 1). By contrast, when a single step of -1×10^{-3} A (*ca.* 7 times more intense current) was applied, the polymerization did not occur (entry 2). This result is consistent with the high (re)generation rate of $[Cu^{I}TREN]^{+}$, resulting therefore in a very high radical concentration at initial stages, which lead to unavoidable and complete termination reactions. To further improve the polymerization, multistep current profiles were introduced (entries 3 and 4), an approach that was demonstrated to be more suitable to achieve better values of $Đ$ and conversion.[52] By choosing appropriate current/time steps, the polymerization significantly improved, affording PVC with relatively low $Đ$ (entry 3). The initiator $CHBr_3$ assured an efficient initiation and simultaneous growth of all PVC chains when appropriate electrolysis program was employed. It is worth mentioning that the elevated values of $Đ$ (compared to other monomers) are usual for RDRP of VC due to the high chain transfer constant and the inevitable formation of some structural defects.[62,82] The best control over the VC polymerization was observed for the multistep electrolysis of 6 hours by applying i_{app} = (−4, −3, −2.5, −1.5 and −1.0) × 10^{-4} A for 300, 600, 2700, 3600 and 14 400 s, respectively. When a multistep program with currents twice these values was used while maintaining the same time intervals, the polymerization became uncontrolled (entry 4) due to the excessive regeneration of activator and the diminished concentration of deactivator species available to quench the growing radicals. Therefore, unless otherwise stated, all further *e*ATRP experiments were conducted using program III. As well as the use of TREN, electrochemical determination of activation rate constant (k_{act}) of the model chain-end 1,1-bromochloroethane by $[Cu^{I}TREN]^{+}$ and its disproportionation rate constant (k_{disp}) revealed that *e*ATRP of VC works because the predominant activator is the active Cu^{I} form of the catalyst. Furthermore, comparing SARA ATRP and *e*ATRP with identical reaction conditions, showed that the latter provides PVC with lower $Đ$ due to the more stringent control over Cu^{I} regeneration (Fig. 7a and section S1, Tables S1 and S2†). This better control and the absence of severe potential drifting is demonstrated by measured evolution of $E_{WE} - E_{CE}$ *vs.* time recorded during *e*ATRPs (Fig. S2–S11†).

Effect of the degree of polymerization

Once a suitable electrolysis program was established (program III, Fig. 7b), the effect of the targeted degree of polymerization

Table 4 *e*ATRP of 50 vol% VC in DMSO, initiated by $CHBr_3$, with different operational conditions at T = 40 °C [a]

Entry	Program	t (h)	M_n^{th}	M_n^{SEC}	$Đ$	Conv. (%)	I_{eff} [b]	$\|Q\|$ [c] (C)
1	I	6	12100	20 700	1.83	40	0.58	3.24
2 [d]	II	6	—	—	—	—	—	21.60
3	III	6	9400	10 900	1.35	31	0.86	2.95
4	IV	6	4800	7100	2.33	16	0.67	5.90

[a] Conversion was determined gravimetrically. Conditions: $C_{VC} : C_{TREN} : C_{Cu} : C_{CHBr_3}$ = 728 : 0.2 : 0.1 : 1.5; V = 10 mL; $C_{Cu} = 10^{-3}$ M, $C_{CHBr_3} = 1.5 \times 10^{-2}$ M. Estimated geometrical surface of the Pt electrode = 6 cm^2. [b] $I_{eff} = M_n^{SEC}/M_n^{th}$. [c] The electric change passed throughout the reaction time. [d] No polymer.

Table 5 *e*ATRP of 50 vol% VC in DMSO, initiated by $CHBr_3$, at different targeted degrees of polymerization at T = 40 °C, catalyzed by $[Cu^{II}TREN]^{2+}$. In the table, DP_T is the targeted DP, while DP is the actual DP ($DP = M_n^{th}/MW^{VC}$)[a]

Entry	DP_T	t (h)	M_n^{th}	M_n^{SEC}	Actual DP	$Đ$	Conv. (%)	I_{eff}	$\|Q\|$ (C)
1	970	6	16 300	13 900	261	1.56	27	0.83	2.95
2	485	6	9400	10 900	150	1.35	31	0.86	2.95
3	243	3	12 100	11 600	194	1.59	80	0.63	1.35

[a] Conversion was determined gravimetrically. Conditions: $C_{VC} : C_{TREN} : C_{Cu} : C_{CHBr_3} = 728 : 0.2 : 0.1 : x$; where x = 0.75, 1.5 and 3.0 for entries 1, 2 and 3, respectively. V = 10 mL; $C_{Cu} = 10^{-3}$ M. Estimated geometrical surface of the Pt electrode = 6 cm^2.

(DP) was studied. The amount of $CHBr_3$ was varied to target different DPs from 243 to 970 (DP_T), keeping all the other reaction parameters constant. The results are summarized in Table 5.

PVC homopolymers ranging from M_n^{SEC} = 10 900 to 13 900 (see SEC traces in Fig. S15†) were obtained by changing $CHBr_3$ concentration. While the conversion settled around 30% for the higher targeted DP_Ts (485 and 970), targeting a lower DP_T = 243 greatly improved conversion, as expected due to the higher radical concentration. Regardless of the DP_T, the results presented in Table 5 suggest the possibility of attaining controlled PVC structures.

Effect of the catalyst concentration

In contrast to SARA ATRP, where C_{Cu} varies slightly with time due to Cu(I) release caused by termination events, in *e*ATRP C_{Cu} is fixed. To test the effect of C_{Cu} a series of *e*ATRPs in which C_{Cu} was progressively diminished, from 1×10^{-3} to 2.5×10^{-4} M, were performed, and the results are summarized in Table 6.

As the catalyst concentration decreased, conversion increased and $Đ$ remained stable, except when $C_{Cu} = 2.5 \times 10^{-4}$ M was used. In this case, there was no appreciable enhancement of conversion while $Đ$ increased significantly. Reducing C_{Cu} while keeping the current feeding constant, forces the catalyst to sustain more activation/deactivation cycles, so that the dormant chain-end is reactivated faster and increases the radical activity time, resulting in the addition of more monomer units (Fig. S16†). When, however, $C_{Cu} = 2.5 \times 10^{-4}$ M is used, almost all Cu^{II} is converted to Cu^{I} to sustain the imposed current, resulting in depletion of the deactivator in the reaction medium. Initiation efficiency (I_{eff}) indeed reflects the depletion and falls as C_{Cu} is decreased.

Effect of the amount of monomer

While PVC is insoluble in its own monomer, similarly to PAN for acrylonitrile,[62] an increase of C_{VC} potentially could improve the polymerization rate to some extent, as apparent propagation rate is linearly dependent on C_{VC}.[1] VC concentration was therefore modulated from 25 to 75 vol%, concurrently reducing the solvent amount. The results are summarized in Table 7.

Reactions in the presence of low and high amounts of VC were limited to 3 hours. The best conditions were found for VC polymerization at 50 vol%, while at 25 and 75%, $Đ$ increased significantly (Fig. S17†).

Effect of the initiator structure

Alkyl halide initiators are critical components for a successful ATRP.[8] Their reactivity, compared to the reactivity of the

Table 6 *e*ATRP of 50 vol% VC in DMSO, initiated by $CHBr_3$, with different $[Cu^{II}TREN]^{2+}$ catalyst concentrations at T = 40 °C[a]

Entry	C_{Cu} (M)	t (h)	M_n^{th}	M_n^{SEC}	$Đ$	Conv. (%)	I_{eff}	$\|Q\|$ (C)
1	10^{-3}	6	9400	10 900	1.35	31	0.86	2.95
2	5×10^{-4}	6	14 200	26 300	1.36	47	0.54	2.95
3	2.5×10^{-4}	6	14 600	26 700	1.76	48	0.55	2.95

[a] Conversion was determined gravimetrically. Conditions: $C_{VC} : C_{TREN} : C_{Cu} : C_{CHBr_3} = 728 : y : x : 1.5$; where x = 0.1, 0.05 and 0.025 for entries 1, 2 and 3, respectively; y = 0.2, 0.1 and 0.5 for entries 1, 2 and 3, respectively. V = 10 mL. Estimated geometrical surface of the Pt electrode = 6 cm^2.

Table 7 *e*ATRP of different vol% VC in DMSO at T = 40 °C, catalyzed by $[Cu^{II}TREN]^{2+}$ [a]

Entry	VC (vol%)	t (h)	M_n^{th}	M_n^{SEC}	$Đ$	Conv. (%)	I_{eff}	$\|Q\|$ (C)
1[b]	25	3	6900	8100	2.40	45	0.85	1.35
2[c]	50	6	9400	10 900	1.35	31	0.86	2.95
3[b]	75	3	5500	20 600	2.74	12	0.27	1.35

[a] Conversion was determined gravimetrically. $C_{VC} : C_{TREN} : C_{Cu} : C_{CHBr_3} = x : 0.2 : 0.1 : 1.5$; where x = 364, 728 and 1093 for entry 1, 2 and 3, respectively; $C_{Cu} = 10^{-3}$ M. V = 10 mL. Estimated geometrical surface of the Pt electrode = 6 cm^2. [b] Electrolysis program V. [c] Electrolysis program III.

dormant species of the polymer, determines the initiation efficiency (I_{eff}) and whether the polymerization is affected by the penultimate effect, *i.e.* a reactivity mismatch between the dormant growing polymer chain and the initiator.[1] Very active initiators such as ethyl α-bromophenylacetate (EBPA) are for example highly recommended in methyl methacrylate polymerization,[96] while methyl 2-bromopropionate (MBP) and ethyl 2-bromoisobutyrate (EBiB) are good initiators for acrylates and monomers less reactive than acrylates (for example acrylamides and styrenes).[8,97,98] The model alkyl halide that mimics VC dormant species is characterized by low activation rate constant ($<10^3$ M^{-1} s^{-1}), therefore even secondary alkyl halides should be good initiators for vinyl chloride polymerization. Electrochemical ATRP of VC was triggered with a series of brominated initiators of different structure (Table 8).

PVC obtained using bromoform and MBP as initiators exhibited molecular weight distribution close to each other with $Đ \leq 1.35$, while with EBiB, $Đ$ was >1.5. Comparing the secondary and tertiary bromides, MBP yielded a much more controlled PVC although of lower molecular weight (Fig. S18†). Therefore, secondary brominated initiators appear to be the best choice for *e*ATRP of VC in terms of control.

Livingness of the polymerization: chain-extension of PVC-Br with MA

To confirm chain-end fidelity, chain-extension of PVC macroinitiators synthesized by *e*ATRP was attempted by both *e*ATRP and SARA ATRP using MA and $[Cu^{II}TREN]^{2+}$ as catalyst. The results are listed in Table 9.

Molecular weight distributions of the macroinitiator and copolymers resulting from chain extensions are shown in Fig. 8.

Chain extension proved that PVC-Br produced by *e*ATRP exhibits living fashion. The macroinitiator was efficiently reactivated using both ATRPs, but the lowest $Đ$ was obtained for *e*ATRP, most probably due to the stringent electrochemical control.

Comparison between *e*ATRP and SARA ATRP with a PVC star architecture

To further expand the toolbox of PVC-based materials and have a wider view of the differences among electrochemical and SARA ATRP, star-shaped PVC was synthetized using the tetra-functional initiator pentaerythritol tetrakis(2-bromoisobutyrate) (EBiB-4f, Scheme 2 and Fig. 9a), as shown in Table 10.

After 3 hours of reaction, *e*ATRP afforded a PVC-Br with higher molecular weight than SARA ATRP, with the same reaction conditions. Sequential activation of the bromoisobutyrate (BriB) functionalities by $[Cu^{I}TREN]^{+}$ allowed the growth of star-shaped PVC ($n^{SEC}_{branch} > 3$). Branching number (n^{SEC}_{branch}) was calculated by the SEC software by Zimm–Stockmayer equations for branching, by selecting star-branched monodisperse case, known the Mark–Houwink–Sakurada parameters for the polymer under analysis (MHS α = 0.517 and $\log K = -2.732$). Among the two polymers, only PVC-Br produced by *e*ATRP exhibits living behavior and adequately narrow molecular weight distribution. Its livingness was verified by chain extension with methyl acrylate (Fig. 9b), to afford the star-shaped copolymer PVC-*b*-PMA-Br.

To prove the livingness of the star-shaped PVC, chain extension by *e*ATRP was attempted with methyl acrylate (Fig. 9b). NMR of the resulting PVC_{765}-*b*-PMA_{193}-Br block copolymer showed the successful formation of the star-shaped structure (Fig. S14†), which in turn resulted of very high $Đ$. Under these conditions, even if PVC-Br macroinitiator is very dilute in the working solution ($C_{PVC\text{-}Br} = 1 \times 10^{-3}$ M), star-star coupling seems inevitable, as seen by a broad shoulder at very high molecular weights ($\log M > 6$). Indeed, calculated hydrodynamic

Table 8 *e*ATRP of 50 vol% VC in DMSO with different brominated initiators at T = 40 °C, catalyzed by $[Cu^{II}TREN]^{2+}$ [a]

Entry	RBr	t (h)	M_n^{th}	M_n^{SEC}	$Đ$	Conv. (%)	I_{eff}	$\lvert Q \rvert$ (C)
1	$CHBr_3$	6	9400	10 900	1.35	31	0.86	2.95
2	EBiB	6	10 300	16 700	1.76	34	0.62	2.95
3	MBP	6	7600	8100	1.26	25	0.94	2.95

[a] Conversion was determined gravimetrically. Conditions $C_{VC} : C_{TREN} : C_{Cu} : C_{RBr} = 728 : 0.2 : 0.1 : 1.5$. V = 10 mL; $C_{Cu} = 10^{-3}$ M. Estimated geometrical surface of the Pt electrode = 6 cm^2.

Table 9 Chain extensions of a PVC macroinitiator by SARA ATRP and *e*ATRP with 50 vol% MA, in DMSO at T = 50 °C, catalyzed by $[Cu^{II}TREN]^{2+}$ [a]

Entry	Method	(Co)polymer	t (h)	M_n^{th}	M_n^{SEC}	$Đ$	Conv. (%)	I_{eff}
1	*e*ATRP	PVC-Br	3	8900	10 600	1.70	29	0.84
2[b]	SARA ATRP	PVC-*b*-PMA-Br	0.16	32 800	34 700	1.59	23	0.94
3[c]	*e*ATRP	PVC-*b*-PMA-Br	0.16	27 000	31 600	1.46	20	0.85

[a] Conversion was determined gravimetrically for ATRP of VC. Conditions for the preparation of macroinitiator by *e*ATRP: $C_{VC} : C_{TREN} : C_{Cu} : C_{CHBr_3} = 728 : 0.2 : 0.1 : 1.5$; electrolysis program V. [b] Conditions chain extension by SARA ATRP: $C_{MA} : C_{TREN} : C_{Cu} : C_{PVC\text{-}Br} = 552 : 0.2 : 0.1 : 0.2$, Cu^0 wire : l = 5 cm, d = 1 mm, DP_T = 2760. [c] Conditions chain extension by *e*ATRP: $C_{MA} : C_{TREN} : C_{Cu} : C_{PVC\text{-}Br} = 552 : 0.2 : 0.1 : 0.2$, estimated Pt area = 6 cm^2, DP_T = 2760, electrolysis program III.

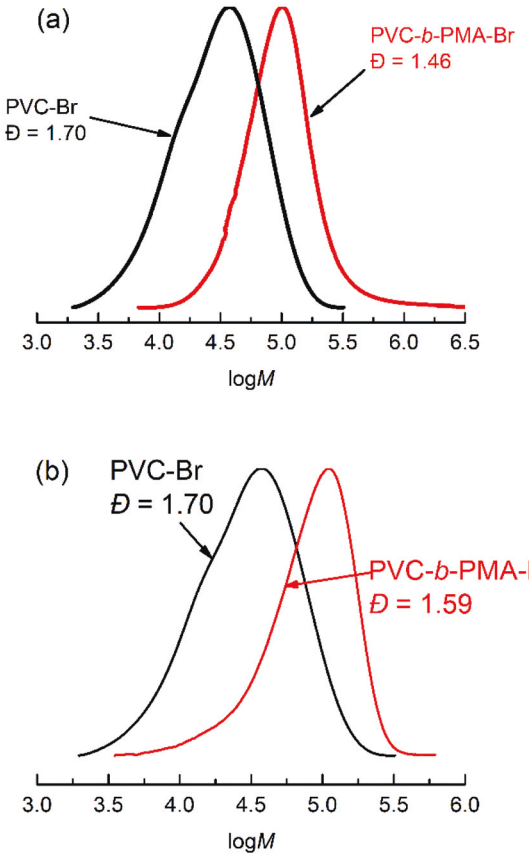

Fig. 8 Molecular weight evolution during the chain extension of a PVC-Br macroinitiator by (a) *e*ATRP and (b) SARA ATRP. All reactions were performed in DMSO at T = 40 °C and catalyzed by $[Cu^{II}TREN]^{2+}$. dn/dc (PVC_{142}) = 0.105, dn/dc (PVC_{142}-*b*-PMA_{278} produced by SARA ATRP) = 0.079 and dn/dc (PVC_{142}-*b*-PMA_{278} produced by *e*ATRP) = 0.073.

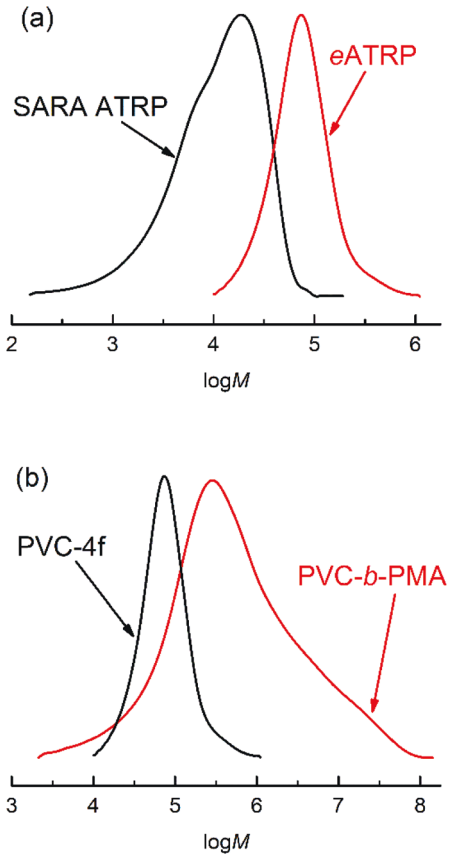

Fig. 9 (a) Molecular weight distributions of star-shaped PVC-Br obtained by SARA ATRP (—) or *e*ATRP (▬) after 3 h of reaction time; (b) chain extensions of a star-shaped PVC-Br macroinitiator obtained by *e*ATRP (—) in the presence of 50 vol% methyl acrylate (▬). All reactions were performed in DMSO at T = 40 °C and catalyzed by $[Cu^{II}TREN]^{2+}$. dn/dc (PVC_{765}-Br) = 0.105, dn/dc (PVC_{765}-*b*-PMA_{193} produced by *e*ATRP) = 0.089.

radius R_h increases from 9.80 nm for the star-shaped PVC homopolymer to 27.48 nm for the star-shaped block copolymer, corresponding to an almost 3-fold increase in size. Mark–Houwink exponent α also passes from 0.517 for the homopolymer (random coil in a good solvent structure) to 0.196 for the star-block copolymer (rigid sphere in an ideal solvent).

Statistical copolymerization of VC

Statistical copolymerization of VC with MA was also attempted, where SARA ATRP and *e*ATRP were again compared. Equimolar amounts of the two monomers (C_{VC} = C_{MA}) were copolymerized, aiming to achieve statistical copolymer of low $Đ$. The results of copolymerization are shown in Table 11.

PVC-*stat*-PMA-Br of narrow molecular weight distributions was obtained when VC was statistically copolymerized with methyl acrylate, at an equimolar ratio (C_{VC} = C_{MA}), with 58% of conversion of monomers (calculated as the sum of VC and MA conversions). In this case, the difference between SARA and *e*ATRP was minimal (Fig. 10). Though, ^{1}H-NMR spectrum of

Table 10 *e*ATRP and SARA ATRP of 50 vol% VC in DMSO using EBiB-4f initiator at T = 40 °C, catalyzed by $[Cu^{II}TREN]^{2+}$ [a]

Entry	Method	t (h)	M_n^{th}	M_n^{SEC}	$Đ$	Conv. (%)	I_{eff}	n_{branch}
1[a]	SARA ATRP	3	5500	5700	2.79	3	0.99	3.8
2[b]	*e*ATRP	3	47 800	54 000	1.79	21	0.88	3.3
3[c]	*e*ATRP	1	64 400	92 000	4.37	7	-	3.3

[a] Conversion was determined gravimetrically for SARA ATRP of VC. Conditions of SARA ATRP: C_{VC} : C_{TREN} : C_{Cu} : $C_{EBiB\text{-}4f}$ = 728 : 0.5 : 0.1 : 0.2; V = 10 mL; C_{Cu} = 10^{-3} M; DP_T = 3640; Cu^0 wire l = 5 cm, d = 1 mm. [b] Conditions of *e*ATRP: C_{VC} : C_{TREN} : C_{Cu} : $C_{EBiB\text{-}4f}$ = 728 : 0.2 : 0.1 : 0.2, V = 10 mL; C_{Cu} = 10^{-3} M; DP_T = 3640; electrolysis program V. [c] Chain extension experiment: C_{MA} : C_{TREN} : C_{Cu} : $C_{PVC\text{-}Br}$ = 552 : 0.2 : 0.1 : 0.1, V = 10 mL, C_{Cu} = 10^{-3} M, DP_T = 5520; electrolysis program III.

Table 11 *e*ATRP and SARA ATRP of 50 vol% MA + VC ($C_{VC} = C_{MA}$) in DMSO using $CHBr_3$ as initiator at T = 40 °C, catalyzed by $[Cu^{II}TREN]^{2+}$ [a]

Entry	Method	t (h)	M_n^{th}	M_n^{SEC}	$Đ$	Comp. ^{PVC} (mol%)	Comp. ^{PMA} (mol%)	I_{eff}	$\|Q\|$ (C)
1	SARA ATRP	6	25 500	21 500	1.42	7	93	1.19	—
2	*e*ATRP	6	20 900	23 700	1.38	8	92	0.88	2.95

[a] Conversion for VC was determined gravimetrically. Conditions of SARA ATRP (entry 1): $C_{VC} : C_{TREN} : C_{Cu} : C_{CHBr_3} = 728 : 0.2 : 0.1 : 1.5$; Cu^0 wire l = 5 cm, d = 1 mm. Conditions of *e*ATRP (entry 2): $C_{VC} : C_{TREN} : C_{Cu} : C_{CHBr_3} = 728 : 0.2 : 0.1 : 1.5$, V = 10 mL; $C_{Cu} = 10^{-3}$ M. DP_T (VC) = 210; DP_T (MA) = 210; electrolysis program III.

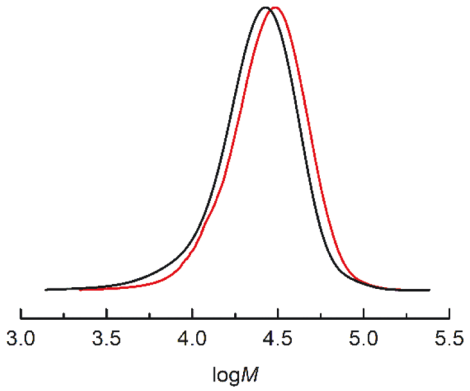

Fig. 10 Molecular weight distributions of PVC-*stat*-PMA-Br obtained by SARA ATRP (—) or *e*ATRP (▬) after 6 h of reaction time in DMSO at T = 40 °C, catalyzed by $[Cu^{II}TREN]^{2+}$.

the copolymer (Fig. S13†) shows that copolymers are essentially composed of PMA with a low incorporation of VC (7 mol%, 1600 g mol^{-1}, ~26 units). This is a consequence of both higher k_{act} and reactivity ratios of MA and VC: (i) PMA-Br chain-end is reactivated faster than PVC-Br and (ii) the high k_p of methyl acrylate (k_p = 24 000 L mol^{-1} s^{-1} in bulk at 60 °C) also favors the homopolymerization rather than the copolymerization.[99,100]

Galvanostatic *e*ATRP of vinyl chloride using the SS304 walls as cathode

*e*ATRP of MA, MMA, Sty and BA can be conveniently triggered, as shown in an earlier work, using the surface of the reactor as a cathode.[52] We investigated the possibility of using the same concept for VC. For this purpose, we replicated the polymerization of Table 4 entry 3, applying to the reactor walls electrolysis program III (see Fig. 7a). The SS304 geometrical area exposed to the solution is ~22 cm^2 or 3.6 times higher than Pt geometrical area. On one hand, modification of electrode area affects the current density (now 3.6 times lower), while on the other the charge applied to the system is still the same. Inevitably, the distribution of the electric field inside the reactor is different and this may affect the polymerization in an unpredictable way. Statistical copolymerization was also attempted with methyl acrylate, replicating the experiment of Table 11 entry 2. The results of this set of experiments are shown in Table 12.

These experiments evidence that PVC can be synthesized by regenerating $[Cu^{I}TREN]^{+}$ on the SS304 walls of the reactor, with or without comonomer. Compared to the same experiment triggered with Pt electrode, $Đ$ and conversions are higher but I_{eff} is lower. It appears that the use of the reactor body as a cathode permits, as for other monomers, the replacement of conventional Pt electrodes. Both polymerizations, in the presence and absence of MA, are controlled. As in the previous case, PVC-*stat*-PMA-Br is essentially composed of PMA with 8 mol% PVC (Fig. 11).

Analysis of the structural defects present in PVC produced by *e*ATRP

As previously mentioned, the high chain transfer causes structural defects in the polymer chain. The most representative and easily detected structural defect for transfer to VC is the –CH═CH–CH_2Cl group. Comparing the signal intensities of hydrogen atoms of PVC backbone –CH_2CHCl– at 4.2–4.6 ppm and the hydrogen atoms of the –CH═CH–CH_2Cl defect structure at 5.8 ppm for CH═CH (Fig. 12) allows quantifying the defect in PVC samples. According to the literature, the –CH_2CHCl–/–CH═CH–CH_2Cl molar ratio is 1000/0.86 for a PVC produced by conventional radical polymerization while this ratio is 1000/0.47 for PVC-Br produced by *e*ATRP (Table 8, entry 3). This result demonstrated less structural defects in the PVC obtained by *e*ATRP, which is also in agreement with other RDRP techniques as NMP[65] and RAFT.[72]

Table 12 *e*ATRP of 50 vol% VC or 50 vol% VC + MA ($C_{VC} = C_{MA}$) in DMSO, using $CHBr_3$ as initiator at T = 40 °C and SS304 walls as cathode, catalyzed by $[Cu^{II}TREN]^{2+}$ [a]

Entry	Monomer(s)	t (h)	M_n^{th}	M_n^{SEC}	$Đ$	Conv. (%)	I_{eff}	$\|Q\|$ (C)
1[b]	VC	6	13 900	27 600	1.61	46	0.50	2.95
2[c]	VC + MA	6	17 700	30 000	1.34	56	0.59	2.95

[a] Conversion was determined gravimetrically, V = 10 mL, $C_{Cu} = 10^{-3}$ M. [b] Conditions: $C_{VC} : C_{TREN} : C_{Cu} : C_{CHBr_3} = 728 : 0.2 : 0.1 : 1.5$. [c] $C_{VC} : C_{MA} : C_{TREN} : C_{Cu} : C_{CHBr_3} = 315 : 315 : 0.2 : 0.1 : 1.5$. DP_T (VC) = 210; DP_T (MA) = 210; electrolysis program III.

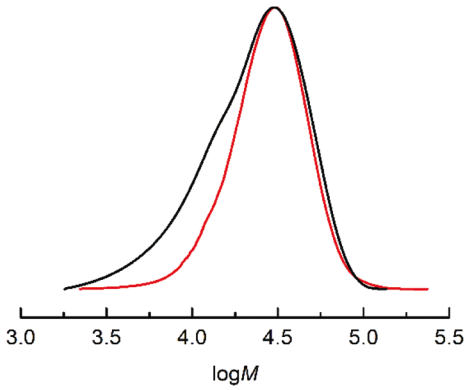

Fig. 11 Molecular weight distributions of PVC-Br (—) and PVC-*stat*-PMA-Br (—) obtained by *e*ATRP after 6 h of reaction time in DMSO at T = 40 °C, catalyzed by $[Cu^{II}TREN]^{2+}$ using the walls of the reactor as cathode.

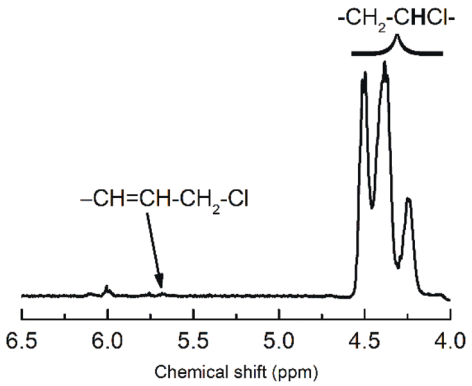

Fig. 12 400 MHz ^{1}H-NMR spectrum of PVC-Br (in the region 4.0–6.5 ppm) produced by *e*ATRP of VC in DMSO at T = 40 °C, initiated by MBP (Table 8, entry 3, M_n = 7600, $Đ$ = 1.26), recorded in THF-d_8 at 25 °C.

Mechanistic consideration on the polymerization of VC mediated by $[Cu^{II}Me_6TREN]^{2+}$: evidence of organometallic trapping

Finally, we were interested to understand why TREN can mediate the polymerization and its derivative Me_6TREN cannot. Although structurally very similar (but with the latter being more sterically hindered by the six CH_3 groups), the two copper catalysts showed a difference as $[BrCu^{II}TREN]^+$ exhibits a standard redox potential more negative than $[BrCu^{II}Me_6TREN]^+$. Thus, TREN complexes are more reducing than Me_6TREN complexes because activity scales with $E_{1/2}$. Nevertheless, experiments showed that complexes of the latter gave no polymerization, both by SARA ATRP and *e*ATRP, which is anomalous at first instance. Therefore, some side reactions could be involved. One possibility is trapping of the poly(vinyl chloride) radicals by Cu(I) catalyst to generate organometallic intermediates R–Cu^{II}/L.[101–104] These species can induce additional catalyzed radical termination (CRT) pathways. Primary radicals form the most stable R–Cu^{II}/L species. The CV of $[Cu^{II}Me_6TREN]^{2+}$ in the presence of 1,1-bromochloroethane was analyzed. This *gem*-dialkyl halide resembles the PVC-Br chain-end and was chosen to mimic the dormant species generated during the early moments of the polymerization. Fig. 13a shows the CV of $[Cu^{II}Me_6TREN]^{2+}$ before (—) and after the addition of 1 eq. of Et_4NBr (—). Fig. 13b shows the CV of $[Cu^{II}Me_6TREN]^{2+}$ after the addition of 2 eq. of $CH_3CHClBr$ at different scan rates, from 0.02 to 0.2 V s^{-1}, while Fig. 13c shows the CV of $[Cu^{II}Me_6TREN]^{2+}$ after the addition of 2 and 4 eq. of $CH_3CHClBr$. The electrochemical response changes in the presence of the model chain-end. Fig. 13a shows a clean shift of CV to more negative values in the presence of bromide anions, as previously reported.[105] The CV in Fig. 13b and c show the formation of a second peak at much more negative potential, as previously stated and assigned to organometallic species $[Cu^{II}(CH_3CHCl)(Me_6TREN)]^+$ ($[R\text{-}Cu^{II}L]^+$).[104,106] Once radicals are formed, they quickly react with $[Cu^{I}Me_6TREN]^+$ to form organometallic species. These organometallic species appear stable for the time scale of a CV (~25 s at the slowest employed scan rate). Such long-time stability of the organometallic species corroborates the inefficient polymerization, as radical trapping is very strong.

It was shown that during MA polymerization, the rate of the OMRP exchange between living and dormant species is at least 10 times slower than that of the ATRP exchange for TPMA-

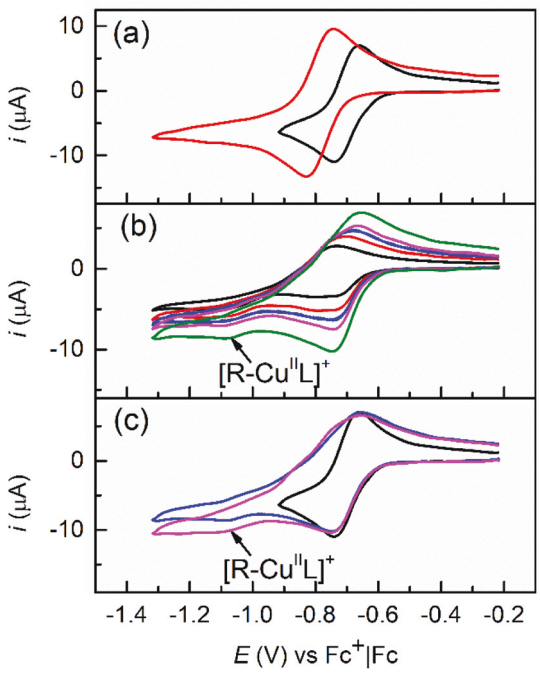

Fig. 13 (a) CV of 10^{-3} M $[Cu^{II}Me_6TREN]^{2+}$ before (—) and after the addition of 1 eq. of Et_4NBr (—); (b) CV of 10^{-3} M $[Cu^{II}Me_6TREN]^{2+}$ after the addition of 2 eq. of $CH_3CHClBr$, at different scan rates, from 0.02 to 0.2 V s^{-1}. (c) CV of 10^{-3} M $[Cu^{II}Me_6TREN]^{2+}$ (—) after the addition of 2 eq. (—) and 4 eq. (—) of $CH_3CHClBr$, recorded at 0.2 V s^{-1}. CV were recorded at a glassy carbon electrode at v = 0.2 V s^{-1} and T = 40 °C in DMSO + 0.1 M Et_4NBF_4.

based ligands.[104] Thus, the main polymerization control is due to the fast ATRP activation/deactivation. However, the presence of organometallics, even if in low quantity, could significantly increase the termination rate of MA in ATRP.[104] The stability of organometallic species (inversely proportional to K_{OMRP}) strongly depends on the degree of substitution of the radical center, following the order 1° > 2° > 3°. Regarding the nature of the radical, the stability depends on the stabilizing groups in the following order: cyano > esters > phenyl. $[Cu^{I}Me_6TREN]^+$ probably traps radicals from VC small oligomers very efficiently, with diffusion controlled rates. CRT therefore appears a serious issue in VC polymerization, at least when catalyzed by Me_6TREN complexes, since K_{ATRP} is low and radicals generated by $CH_3CHClBr$ activation are secondary radicals. The contribution of CRT can be diminished by increasing the ATRP activity, *i.e.* passing for example from Me_6TREN to TREN. Considering these results, we assume that the polymerization of vinyl chloride is significantly hampered by formation of organometallic species in the presence of Cu/Me_6TREN but not with Cu/TREN.

Conclusions

The use of $[Cu^{II}TREN]^{2+}$ as the only efficient catalyst for VC polymerization, resulted in the successful synthesis of PVC by *e*ATRP. It is important to note that due to the absence of metallic copper wire/powder, only $[Cu^{I}TREN]^+$ is the activator, so that the polymerization of vinyl chloride proceeds without the aid of Cu^0. During the polymerizations three major constraints have been recognized: (1) the gaseous nature of vinyl chloride requires a dedicated equipment and implies operative constrictions. Furthermore, this monomer has a very high chain transfer constant, compared to acrylates or methacrylates and affects the behavior of the polymerization; (2) the dynamic activation/deactivation equilibrium, mediated by the catalyst, plays a significant role in governing dispersity. However, we found only one ligand (TREN) that forms a catalyst able to successfully mediate the polymerization. This restriction limits the possibility of optimization by exploiting other catalysts that potentially could have a more positive impact on dispersity; (3) traditional electrodes/glassware could not be used, including reference electrodes. Without the reference electrode, we had to operate *via* a different approach, applying current steps letting the potential free to drift. Vinyl chloride was polymerized by *e*ATRP using down to 140 ppm of copper complex with respect to the monomer, resulting in up to 80% VC conversion in 3 hours at T = 40 °C (yielding PVC with M_n^{SEC} in good agreement with theoretical values and $Đ$ = 1.30–1.70). The polymerization was also studied by changing catalyst and monomer loading, DP, ligand, and alkyl bromide initiators. The living behavior of the polymer was demonstrated by the ability to reactivate dormant PVC-Br, produced by *e*ATRP, through chain-extension with methyl acrylate, by using both *e*ATRP and SARA ATRP. PVC-*b*-PMA block copolymers with both linear and star shaped architectures were synthesized; the latter, however, was contaminated by star-star coupling. PVC and its copolymers were also obtained by regenerating $[Cu^{I}TREN]^+$ on the SS304 scaffold of the reactor, without the need of expensive Pt electrodes, showing the exceptional versatility and robustness of electrochemical polymerization methods even using bulk non-noble electrodes.

Conflicts of interest

The authors declare no competing financial interest.

Acknowledgements

The authors thank University of Padova for the financial support. Francesco De Bon thanks Fondazione "Ing. Aldo Gini" for the financial support and Fondazione Cariparo for his PhD grant. Francesco De Bon and Diana C. M. Ribeiro acknowledge FCT for the project POCI-01-0145-FEDER-029742 (POLYCEL). Funding from MATIS (CENTRO-01-0145-FEDER-000014), co-financed by the European Regional Development Fund (FEDER) through "Programa Operacional Regional do Centro" (CENTRO2020) is acknowledged. Carlos M. R. Abreu wishes to thank Fundação para a Ciência e Tecnologia (FCT) through the Scientific Employment Stimulus 2018 (CEECIND/03591/2018) and Agência Nacional de Inovação through the Project VinylGreen (QREN 17798), for the financial support. Krzysztof Mayjaszewski acknowledges NSF CHE 2000391. The authors greatly acknowledge Prof. Christopher M. A. Brett for offering his electrochemical equipment for this work and M. Santos for the graphics. The NMR data were obtained at the Nuclear Magnetic Resonance Laboratory of the Coimbra Chemistry Centre (http://www.nmrccc.uc.pt), University of Coimbra, supported in part by Grant REEQ/481/QUI/2006 from FCT, POCI-2010, and FEDER, Portugal. This research was partially sponsored by FEDER funds through the program COMPETE – Programa Operacional Factores de Competitividade – and by national funds through FCT – Fundação para a Ciência e a Tecnologia, under the project UID/00285/2020.

Notes and references

1 X. Pan, M. Fantin, F. Yuan and K. Matyjaszewski, *Chem. Soc. Rev.*, 2018, **47**, 5457–5490.
2 K. Matyjaszewski, *Adv. Mater.*, 2018, **30**, e1706441.
3 F. Seeliger and K. Matyjaszewski, *Macromolecules*, 2009, **42**, 6050–6055.
4 J. Mosnáček and K. Matyjaszewski, *Macromolecules*, 2008, **41**, 5509–5511.
5 P. Kwiatkowski, J. Jurczak, J. Pietrasik, W. Jakubowski, L. Mueller and K. Matyjaszewski, *Macromolecules*, 2008, **41**, 1067–1069.
6 T. Arita, Y. Kayama, K. Ohno, Y. Tsujii and T. Fukuda, *Polymer*, 2008, **49**, 2426–2429.

7 W.-M. Wan and C.-Y. Pan, *Macromolecules*, 2007, **40**, 8897–8905.
8 W. Tang and K. Matyjaszewski, *Macromolecules*, 2007, **40**, 1858–1863.
9 W. Jakubowski, K. Min and K. Matyjaszewski, *Macromolecules*, 2006, **39**, 39–45.
10 W. Jakubowski and K. Matyjaszewski, *Angew. Chem.*, 2006, **118**, 4594–4598.
11 D. Neugebauer and K. Matyjaszewski, *Macromolecules*, 2003, **36**, 2598–2603.
12 S. B. Lee, A. J. Russell and K. Matyjaszewski, *Biomacromolecules*, 2003, **4**, 1386–1393.
13 N. V. Tsarevsky, T. Sarbu, B. Göbelt and K. Matyjaszewski, *Macromolecules*, 2002, **35**, 6142–6148.
14 S. Traian, P. Tomislav, M. Blayne and M. Krzysztof, *J. Polym. Sci., Part A: Polym. Chem.*, 2002, **40**, 3153–3160.
15 K. L. Robinson, M. A. Khan, M. V. de Paz Báñez, X. S. Wang and S. P. Armes, *Macromolecules*, 2001, **34**, 3155–3158.
16 J. T. Rademacher, M. Baum, M. E. Pallack, W. J. Brittain and W. J. Simonsick, *Macromolecules*, 2000, **33**, 284–288.
17 J. Xia, X. Zhang and K. Matyjaszewski, *Macromolecules*, 1999, **32**, 3531–3533.
18 M. Teodorescu and K. Matyjaszewski, *Macromolecules*, 1999, **32**, 4826–4831.
19 K. A. Davis, H.-j. Paik and K. Matyjaszewski, *Macromolecules*, 1999, **32**, 1767–1776.
20 J. Xia, S. G. Gaynor and K. Matyjaszewski, *Macromolecules*, 1998, **31**, 5958–5959.
21 K. Matyjaszewski, T. E. Patten and J. Xia, *J. Am. Chem. Soc.*, 1997, **119**, 674–680.
22 Y. Wang, M. Fantin and K. Matyjaszewski, *J. Polym. Sci., Part A: Polym. Chem.*, 2018, **57**, 376–381.
23 J.-K. Guo, Y.-N. Zhou and Z.-H. Luo, *AIChE J.*, 2018, **64**, 961–969.
24 P. Chmielarz, M. Fantin, S. Park, A. A. Isse, A. Gennaro, A. J. D. Magenau, A. Sobkowiak and K. Matyjaszewski, *Prog. Polym. Sci.*, 2017, **69**, 47–78.
25 M. Fantin, S. Park, Y. Wang and K. Matyjaszewski, *Macromolecules*, 2016, **49**, 8838–8847.
26 S. Park, P. Chmielarz, A. Gennaro and K. Matyjaszewski, *Angew. Chem., Int. Ed.*, 2015, **54**, 2388–2392.
27 P. Chmielarz, S. Park, A. Simakova and K. Matyjaszewski, *Polymer*, 2015, **60**, 302–307.
28 B. Li, B. Yu, W. T. Huck, W. Liu and F. Zhou, *J. Am. Chem. Soc.*, 2013, **135**, 1708–1710.
29 A. J. D. Magenau, N. C. Strandwitz, A. Gennaro and K. Matyjaszewski, *Science*, 2011, **332**, 81–84.
30 N. Bortolamei, A. A. Isse, A. J. D. Magenau, A. Gennaro and K. Matyjaszewski, *Angew. Chem.*, 2011, **123**, 11593–11596.
31 L. Mueller, W. Jakubowski, K. Matyjaszewski, J. Pietrasik, P. Kwiatkowski, W. Chaladaj and J. Jurczak, *Eur. Polym. J.*, 2011, **47**, 730–734.
32 J. Morick, M. Buback and K. Matyjaszewski, *Macromol. Chem. Phys.*, 2012, **213**, 2287–2292.
33 H. Schroeder, M. Buback and K. Matyjaszewski, *Macromol. Chem. Phys.*, 2014, **215**, 44–53.
34 Y. Wang, H. Schroeder, J. Morick, M. Buback and K. Matyjaszewski, *Macromol. Rapid Commun.*, 2013, **34**, 604–609.
35 M. Horn and K. Matyjaszewski, *Macromolecules*, 2013, **46**, 3350–3357.
36 W. Tang and K. Matyjaszewski, *Macromolecules*, 2006, **39**, 4953–4959.
37 X. Zheng, Q. Liu, M. Li, W. Feng, H. Yang and J. Kong, *Bioelectrochemistry*, 2020, 107462, DOI: 10.1016/j.bioelechem.2020.107462.
38 A. Michieletto, F. Lorandi, F. De Bon, A. A. Isse and A. Gennaro, *J. Polym. Sci.*, 2019, **58**, 114–123.
39 J.-K. Guo, Y.-N. Zhou and Z.-H. Luo, *Chem. Eng. J.*, 2019, **372**, 163–170.
40 J. Wang, M. Tian, S. Li, R. Wang, F. Du and Z. Xue, *Polym. Chem.*, 2018, **9**, 4386–4394.
41 Q. Liu, K. Ma, D. Wen, Q. Wang, H. Sun, Q. Liu and J. Kong, *J. Electroanal. Chem.*, 2018, **823**, 20–25.
42 D. Li, J. Wu, S. Yang, W. Zhang and F. Ran, *New J. Chem.*, 2017, **41**, 9918–9930.
43 Y. Hu, B. Liang, L. Fang, G. Ma, G. Yang, Q. Zhu, S. Chen and X. Ye, *Langmuir*, 2016, **32**, 11763–11770.
44 J.-K. Guo, Y.-N. Zhou and Z.-H. Luo, *Macromolecules*, 2016, **49**, 4038–4046.
45 Y. Sun, H. Du, Y. Deng, Y. Lan and C. Feng, *J. Solid State Electrochem.*, 2015, **20**, 105–113.
46 N. Shida, Y. Koizumi, H. Nishiyama, I. Tomita and S. Inagi, *Angew. Chem., Int. Ed.*, 2015, **54**, 3922–3926.
47 P. Chmielarz, A. Sobkowiak and K. Matyjaszewski, *Polymer*, 2015, **77**, 266–271.
48 B. Li, B. Yu and F. Zhou, *Macromol. Rapid Commun.*, 2013, **34**, 246–250.
49 B. Li, B. Yu, W. T. Huck, F. Zhou and W. Liu, *Angew. Chem., Int. Ed.*, 2012, **51**, 5092–5095.
50 A. J. D. Magenau, N. Bortolamei, E. Frick, S. Park, A. Gennaro and K. Matyjaszewski, *Macromolecules*, 2013, **46**, 4346–4353.
51 F. De Bon, A. A. Isse and A. Gennaro, *ChemElectroChem*, 2019, **6**, 4257–4265.
52 F. De Bon, A. A. Isse and A. Gennaro, *Electrochim. Acta*, 2019, **304**, 505–512.
53 E. Trevisanello, F. De Bon, G. Daniel, F. Lorandi, C. Durante, A. A. Isse and A. Gennaro, *Electrochim. Acta*, 2018, **285**, 344–354.
54 F. De Bon, M. Fantin, A. A. Isse and A. Gennaro, *Polym. Chem.*, 2018, **9**, 646–655.
55 M. Fantin, F. Lorandi, A. A. Isse and A. Gennaro, *Macromol. Rapid Commun.*, 2016, **37**, 1318–1322.
56 F. Lorandi, M. Fantin, A. A. Isse and A. Gennaro, *Polym. Chem.*, 2016, **7**, 5357–5365.
57 A. Debuigne, C. Jérôme and C. Detrembleur, *Polymer*, 2017, **115**, 285–307.
58 K. Parkatzidis, H. S. Wang, N. P. Truong and A. Anastasaki, *Chem*, 2020, **6**, 1575–1588.

59 C. Barner-Kowollik, S. Beuermann, M. Buback, P. Castignolles, B. Charleux, M. L. Coote, R. A. Hutchinson, T. Junkers, I. Lacík, G. T. Russell, M. Stach and A. M. van Herk, *Polym. Chem.*, 2014, **5**, 204–212.
60 X. Yu, J. Pfaendtner and L. J. Broadbelt, *J. Phys. Chem. A*, 2008, **112**, 6772–6782.
61 J. Ugelstad, P. Mork, F. Hansen, K. Kaggerud and T. Ellingsen, *Pure Appl. Chem.*, 1981, **53**, 323–363.
62 C. M. R. Abreu, A. C. Fonseca, N. M. P. Rocha, J. T. Guthrie, A. C. Serra and J. F. J. Coelho, *Prog. Polym. Sci.*, 2018, **87**, 34–69.
63 V. Percec, A. V. Popov, E. Ramirez-Castillo, J. F. J. Coelho and L. A. Hinojosa-Falcon, *J. Polym. Sci., Part A: Polym. Chem.*, 2004, **42**, 6267–6282.
64 Y. Piette, A. Debuigne, C. Jérôme, V. Bodart, R. Poli and C. Detrembleur, *Polym. Chem.*, 2012, **3**, 2880.
65 C. M. R. Abreu, P. V. Mendonca, A. C. Serra, B. B. Noble, T. Guliashvili, J. Nicolas, M. L. Coote and J. F. J. Coelho, *Macromolecules*, 2016, **49**, 490–498.
66 C. M. R. Abreu, P. Maximiano, T. Guliashvili, J. Nicolas, A. C. Serra and J. F. J. Coelho, *RSC Adv.*, 2016, **6**, 7495–7503.
67 J. P. Mendes, J. R. Góis, J. R. C. Costa, P. Maximiano, A. C. Serra, T. Guliashvili and J. F. J. Coelho, *J. Polym. Sci., Part A: Polym. Chem.*, 2017, **55**, 1322–1328.
68 J. P. Mendes, P. V. Mendonca, P. Maximiano, C. M. R. Abreu, T. Guliashvili, A. C. Serra and J. F. J. Coelho, *RSC Adv.*, 2016, **6**, 9598–9603.
69 J. P. Mendes, F. Branco, C. M. R. Abreu, P. V. Mendonça, A. C. Serra, A. V. Popov, T. Guliashvili and J. F. J. Coelho, *ACS Macro Lett.*, 2014, **3**, 858–861.
70 P. Maximiano, J. P. Mendes, P. V. Mendonca, C. M. R. Abreu, T. Guliashvili, A. C. Serra and J. F. J. Coelho, *J. Polym. Sci., Part A: Polym. Chem.*, 2015, **53**, 2722–2729.
71 P. V. Mendonça, J. P. M. Ribeiro, C. M. R. Abreu, T. Guliashvili, A. C. Serra and J. F. J. Coelho, *ACS Macro Lett.*, 2019, **8**, 315–319.
72 C. M. R. Abreu, P. V. Mendonça, A. C. Serra, J. F. J. Coelho, A. V. Popov, G. Gryn'ova, M. L. Coote and T. Guliashvili, *Macromolecules*, 2012, **45**, 2200–2208.
73 C. M. R. Abreu, T. C. Rezende, A. C. Fonseca, T. Guliashvili, C. Bergerbit, F. D'Agosto, L.-J. Yu, A. C. Serra, M. L. Coote and J. F. J. Coelho, *Macromolecules*, 2020, **53**, 190–202.
74 T. Hatano, B. M. Rosen and V. Percec, *J. Polym. Sci., Part A: Polym. Chem.*, 2010, **48**, 164–172.
75 M. J. Sienkowska, B. M. Rosen and V. Percec, *J. Polym. Sci., Part A: Polym. Chem.*, 2009, **47**, 4130–4140.
76 V. Percec, T. Guliashvili, J. S. Ladislaw, A. Wistrand, A. Stjerndahl, M. J. Sienkowska, M. J. Monteiro and S. Sahoo, *J. Am. Chem. Soc.*, 2006, **128**, 14156–14165.
77 V. Percec, A. V. Popov, E. Ramirez-Castillo and O. Weichold, *J. Polym. Sci., Part A: Polym. Chem.*, 2003, **41**, 3283–3299.
78 A. D. Asandei and V. Percec, *J. Polym. Sci., Part A: Polym. Chem.*, 2001, **39**, 3392–3418.
79 J. F. J. Coelho, A. C. Fonseca, J. R. Gois, P. M. O. F. Gonçalves, A. V. Popov and M. H. Gil, *Chem. Eng. J.*, 2011, **169**, 399–413.
80 J. F. J. Coelho, P. M. F. O. Gonçalves, D. Miranda and M. H. Gil, *Eur. Polym. J.*, 2006, **42**, 751–763.
81 B. Iván, in *Polymer Durability*, American Chemical Society, 1996, vol. 249, ch. 2, pp. 19–32.
82 W. H. Starnes, *Prog. Polym. Sci.*, 2002, **27**, 2133–2170.
83 T. C. Rezende, C. M. R. Abreu, A. C. Fonseca, C. M. Higa, L. Li, A. C. Serra, R. Braslau and J. F. J. Coelho, *Polymer*, 2020, **196**, 122473.
84 P. Krys, Y. Wang, K. Matyjaszewski and S. Harrisson, *Macromolecules*, 2016, **49**, 2977–2984.
85 D. Konkolewicz, P. Krys, J. R. Góis, P. V. Mendonça, M. Zhong, Y. Wang, A. Gennaro, A. A. Isse, M. Fantin and K. Matyjaszewski, *Macromolecules*, 2014, **47**, 560–570.
86 D. Konkolewicz, Y. Wang, M. J. Zhong, P. Krys, A. A. Isse, A. Gennaro and K. Matyjaszewski, *Macromolecules*, 2013, **46**, 8749–8772.
87 L. Falciola, A. Gennaro, A. A. Isse, P. R. Mussini and M. Rossi, *J. Electroanal. Chem.*, 2006, **593**, 47–56.
88 V. Percec, A. V. Popov, E. Ramirez-Castillo, M. Monteiro, B. Barboiu, O. Weichold, A. D. Asandei and C. M. Mitchell, *J. Am. Chem. Soc.*, 2002, **124**, 4940–4941.
89 B. M. Rosen and V. Percec, *Chem. Rev.*, 2009, **109**, 5069–5119.
90 M. E. Levere, N. H. Nguyen, X. Leng and V. Percec, *Polym. Chem.*, 2013, **4**, 1635–1647.
91 W. G. Skene, J. C. Scaiano, N. A. Listigovers, P. M. Kazmaier and M. K. Georges, *Macromolecules*, 2000, **33**, 5065–5072.
92 P. De Paoli, A. A. Isse, N. Bortolamei and A. Gennaro, *Chem. Commun.*, 2011, **47**, 3580–3582.
93 F. Lorandi, M. Fantin, A. A. Isse and A. Gennaro, *Polymer*, 2015, **72**, 238–245.
94 F. Lorandi, M. Fantin, F. De Bon, A. A. Isse and A. Gennaro, in *Reversible Deactivation Radical Polymerization: Mechanisms and Synthetic Methodologies*, American Chemical Society, 2018, vol. 1284, ch. 7, pp. 161–189.
95 C. M. R. Abreu, A. C. Fonseca, N. M. P. Rocha, J. T. Guthrie, A. C. Serra and J. F. J. Coelho, in *Reversible Deactivation Radical Polymerization: Mechanisms and Synthetic Methodologies*, American Chemical Society, 2018, vol. 1284, ch. 10, pp. 227–261.
96 K. F. Augustine, T. G. Ribelli, M. Fantin, P. Krys, Y. Cong and K. Matyjaszewski, *J. Polym. Sci., Part A: Polym. Chem.*, 2017, **55**, 3048–3057.
97 C. Fang, M. Fantin, X. Pan, K. de Fiebre, M. L. Coote, K. Matyjaszewski and P. Liu, *J. Am. Chem. Soc.*, 2019, **141**, 7486–7497.
98 F. Lorandi, F. De Bon, M. Fantin, A. A. Isse and A. Gennaro, *Electrochem. Commun.*, 2017, **77**, 116–119.

99 T. Fukuda, A. Goto and Y. Tsujii, in *Handbook of Radical Polymerization*, ed. K. Matyjaszewski and T. P. Davis, John Wiley and sons, 2002, pp. 407–462, DOI: 10.1002/0471220450.ch9.
100 M. L. Coote and T. P. Davis, in *Handbook of Radical Polymerization*, ed. K. Matyjaszewski and T. P. Davis, John Wiley and sons, 2002, pp. 263–300, DOI: 10.1002/0471220450.ch5.
101 K. Schröder, D. Konkolewicz, R. Poli and K. Matyjaszewski, *Organometallics*, 2012, **31**, 7994–7999.
102 N. Soerensen, H. Schroeder and M. Buback, *Macromolecules*, 2016, **49**, 4732–4738.
103 T. G. Ribelli, S. M. Wahidur Rahaman, J.-C. Daran, P. Krys, K. Matyjaszewski and R. Poli, *Macromolecules*, 2016, **49**, 7749–7757.
104 M. Fantin, F. Lorandi, T. G. Ribelli, G. Szczepaniak, A. E. Enciso, C. Fliedel, L. Thevenin, A. A. Isse, R. Poli and K. Matyjaszewski, *Macromolecules*, 2019, **52**, 4079–4090.
105 N. Bortolamei, A. A. Isse, V. B. Di Marco, A. Gennaro and K. Matyjaszewski, *Macromolecules*, 2010, **43**, 9257–9267.
106 L. Thevenin, C. Fliedel, M. Fantin, T. G. Ribelli, K. Matyjaszewski and R. Poli, *Inorg. Chem.*, 2019, **58**, 6445–6457.